Freezing-thawing of porous media

An extended finite element approach for soil freezing and thawing

Arzanfudi, Mehdi Musivand; Al-Khoury, Rafid

DOI
10.1016/j.advwatres.2018.07.013

Publication date
2018

Document Version
Accepted author manuscript

Published in
Advances in Water Resources

Citation (APA)
Arzanfudi, M. M., & Al-Khoury, R. (2018). Freezing-thawing of porous media: An extended finite element approach for soil freezing and thawing. *Advances in Water Resources*, *119*, 210-226. https://doi.org/10.1016/j.advwatres.2018.07.013

Freezing-Thawing of Porous Media: an Extended Finite Element Approach for Soil Freezing and Thawing

Mehdi Musivand Arzanfudi* and Rafid Al-Khoury

Faculty of Civil Engineering and Geosciences, Delft University of Technology, P.O. Box 5048, 2600 GA Delft, The Netherlands

Abstract

This paper introduces a thermo-hydro-mechanical computational model for freezing and thawing in porous media domains, with focus on freezing and thawing in soil. The model is formulated based on the averaging theory and discretized using a mixed discretization scheme, where the standard and extended finite element methods are simultaneously employed. It is capable of capturing the strong coupling between all important phenomena and processes occurring during relatively high freezing-thawing rates in porous media. Solid and fluid compressibility, buoyancy, phase change, thermomechanical behavior, water volume change, pores expansion, cryogenic suction, melting point depression and water migration to the freezing zone are all considered in the model. The cryogenic suction, in particular, is central to the occurrence of many of these phenomena and processes, and thus treated as a primary state variable, and discretized using the partition of unity method to make sure that it can be captured accurately. The paper presents detailed formulation of the governing equations and the numerical discretization. Verification and numerical examples are given to demonstrate the accuracy and computational capability of the model in describing the behavior of a soil mass subjected to boundary conditions resembling those occurring in the vicinity of an energy pile. The numerical examples show that the model is effectively mesh-independent and can simulate all important phenomena using relatively coarse meshes.

Keywords: freezing-thawing in soil, energy pile, cryogenic suction, cryosuction, THM model, melting point depression, ice lens.

1 Introduction

Freezing of water in porous media is a natural phenomenon which is of interest in a wide range of engineering applications, including geotechnical engineering, environmental engineering, soil physics, food industry and biomechanics, just to name a few. This paper focuses on freezing and thawing in soil, though the model is generic and can readily be adopted for other applications. In particular, it focuses on freezing and thawing of soil in the vicinity of energy piles (Anstett et al. 2005). The energy

* Corresponding author: Mehdi Musivand Arzanfudi
Faculty of Civil Engineering and Geosciences, Delft University of Technology, P.O. Box 5048, 2600 GA Delft, The Netherlands. Tel.: +31 (0)15 27 88216
E-mail: M.MusivandArzanfudi@tudelft.nl

pile is a new shallow geothermal technology that utilizes the foundation piles as heat exchangers for heating and cooling of buildings. Normally, users of this technology are restricted by operating the energy system to temperatures well above water freezing point to ensure that no thermally-induced damages occur to the piles and the soil-pile interaction. However, this restriction would significantly limit the amount of energy that can be extracted from the earth. The goal of this work is to extend the operational limits of the system by studying the scenarios that might occur due to freezing and thawing of the soil mass and their consequences on the pile, and provide the criteria for operating the energy piles at temperatures below the freezing point. This paper is a step towards this goal. It introduces a computational model describing freezing and thawing in a soil mass subjected to boundary conditions resembling those occurring in energy pile applications.

Water freezing in porous media has been extensively studied experimentally and theoretically. Experimental studies have demonstrated that porous materials at temperatures well below freezing point preserve significant amount of unfrozen liquid water in their pores. This characteristic is hypothesized to be attributed to two mechanisms: interfacial premelting and curvature-induced premelting (Wettlaufer and Worster 2006). The interfacial premelting gives rise to an unfrozen thin film of liquid water at the contact surface between the ice crystals and the solid particles. The curvature-induced premelting generates supercooled pore water arising from the crystal ice surface curvature. Normally, the premelting mechanisms are negligible in many applications, but, in soil, as the specific surface area can be remarkably high and the surface curvature can be small, these mechanisms can sum up to a significant amount of unfrozen water, leading to what is known as the melting point depression.

The melting point depression in porous media is associated with the development of thermally-induced negative pore pressure, known as cryogenic suction (Williams and Smith 1991), also denoted as cryosuction. Negative pore pressure of 11 to 12 atm generates from every degree Celsius below zero. The cryogenic suction gives rise to water migration from the unfrozen region to the frozen region. The migrated water can create pockets where it amalgamates to form ice lens. This phenomenon is important in permafrost regions like Arctic and Antarctic, but for an energy pile application it is of minor significance. However, laboratory experiments on soil samples have shown that segregated ice lenses are generated in the frozen zone (Ming et al. 2016; Steiner et al. 2017). Formation of the ice lenses and migration of water to the frozen region lead to expansion of porosity, giving rise to frost heaving. The amount of frost heaving in a porous domain depends, among others, on the temperature gradient, overburden pressure, soil stiffness and the thermodynamic properties of water. Water, in particular, exhibits some unique abnormalities; its specific volume above 4°C decreases with decreasing temperature down to 4°C, below which, unlike other materials, its specific volume increases with decreasing temperature.

Apparently, soil freezing is a complicated phenomenon which encompasses highly coupled processes associating premelting to generation of cryogenic suction to expansion of porosity to formation of ice lenses to frost heaving. Upon thawing these processes undergo reversing action

manifested by the diminishing of cryogenic suction, retreating of water to its initial equilibrium condition and reversing the frost heaving to become thawing settlement. Evidently, this strong coupling between thermal, hydraulic and mechanical behavior in response to freezing and thawing necessitates considering all aforementioned processes in the model. Besides, the significance of these processes is considerably affected by the geometry of the problem, the gravitational forces and the material characteristics, and hence, the use of proper constitutive relationships and advanced numerical discretization schemes are essential.

Attempts to model freezing and thawing in soil can be categorized into three types of models: thermo-hydraulic (TH) models; thermo-mechanical (TM) models; and thermo-hydro-mechanical (THM) models. The TH models are formulated based on the conservation of mass and energy equations, with no regard given to the linear momentum (equilibrium) equation of the solid matrix. Models introduced by Harlan (1973), Guymon and Luthin (1974), Takagi (1979), Gilpin (1980), O'Neill and Miller (1985), Konrad and Duquennoi (1993), and Sheng et al. (1995) are among the TH category. The TM models are formulated based on the conservation of energy and linear momentum equations, with no regard given to the fluid mass conservation equation. The model introduced by Kruschwitz and Bluhm (2005), for instance, is among the TM category. Models of this category ignore the cryogenic suction and its associated water mass migration to the frozen zone. The THM models are formulated based on the conservation of mass, energy and linear momentum equations. Models introduced by Mikkola and Hartikainen (2001), Nishimura et al. (2008), Thomas et al. (2009), and Ming et al. (2016) are among this category. These models simulate soil freezing with different level of complexities, with a noteworthy work given by Zhou and Meschke (2013), who introduced a THM model based on the theory of thermo-poro-elasticity of Coussy (2005) and the theory of premelting dynamics of Wettlaufer and Worster (2006). The essence of this work is in the use of entropy for deriving the constitutive relationships of the materials.

The aforementioned models have been formulated based on the finite difference, finite volume and finite element methods. The focus was on simulating the physics of the problem, and mainly standard discretization procedures have been employed to describe the primary state variables. As a consequence, these models entail the use of fine grids, mainly if the freezing rate is high and the cryogenic suction is of interest. Nevertheless, recent works on soil freezing focus also on the numerical procedure. Bekele et al. (2017) presented an isogeometric finite element model for modeling artificial ground freezing. This technique makes use of the computer-aided design (CAD) basis functions to formulate the finite elements, which characteristically have better capabilities in describing the geometry. Na and Sun (2017) introduced a stabilized finite element model for freezing and thawing of an elasto-plastic porous domain. They adopt a stabilization technique to counteract the lack of two-fold inf–sup condition and ill-conditioning due to using primary state variables of different nature to prevent the likely occurrences of spurious oscillations. Recently, Amiri et al. (2018) introduced a TH model using the extended finite element method (XFEM) to model the temperature discontinuity at the ice/water interface.

In this work, focus is placed on both, the physics of the problem and the computational efficiency of the model. Compared to all existing works, this work is distinct by three main features: 1) the comprehensive mathematical formulation of the physics, and the generic employment of the constitutive relationships; 2) the choice of the primary state variables; and 3) the use of the partition of unity to discretize the cryogenic suction. These features and their novelty are highlighted in Section 2. In Section 3, details of the governing equations, including the conservation equations, constitutive relationships, and initial and boundary conditions are given. A step-by-step mixed finite element discretization scheme is presented in Section 4. A partial verification exercise describing the model accuracy in simulating a numerical thawing benchmark case is given in Section 5. Section 6 presents a numerical example, highlighting the complete features of the model. The conclusions of this work are outlined in Section 7. Appendices A-C provide additional details, including the water equation of state (EOS), the linearized equations, and the complete components of finite element matrices and vectors.

2 Modeling approach

Developing an accurate, efficient and effectively mesh-independent model for freezing and thawing in deformable porous media requires a well-designed conceptual model, a descriptive mathematical formulation, a good choice of the primary state variables and a well-suited numerical method.

We undertake a conceptual model that comprises a saturated, three-phase deformable porous medium domain subjected to relatively high freezing-thawing rates boundary conditions. The porous domain constitutes a solid phase (porous matrix) and water, which can be in a liquid phase, ice phase, or a mixture. The conceptual model incorporates all important physical and thermodynamic phenomena and processes occurring during freezing and thawing in porous media, including solid and fluid compressibility, buoyancy, phase change, thermomechanical behavior, pore volume expansion, water volume change, cryogenic suction, melting point depression and water migration to the freezing zone.

The balance equations are formulated based on the representative elementary volume (REV) averaging theory (Lewis and Schrefler 1998). Phenomenological constitutive relationships and equations of state are employed for the solid and water phases. The solid phase is considered temperature-dependent elastic, with its modulus of elasticity being a function of temperature. The water equation of state is adopted from the International Association for the Properties of Water and Steam (IAPWS 2007). The water and ice thermal expansion, heat conductivity and dynamic viscosity are considered functions of temperature. The Clausius-Clapeyron relation, describing the thermodynamic equilibrium between the frozen and unfrozen water contents in the porous domain, is utilized to describe the cryogenic suction. An empirical relationship describing the melting point depression is formulated. Water flow is governed by Darcy's law, and the relative permeability of the liquid water is described using the Brooks and Corey (1964) relationship.

Appropriate choice of the primary state variables is very important for obtaining a stable numerical scheme. As indicated above, the conceptual model encompasses all important features involved in

freezing and thawing of a porous domain constituting a solid phase, liquid water phase, ice phase and a water mixture. As it will be apparent later on this paper, the governing equations contain 21 mechanical and thermodynamic state variables describing the thermo-hydro-mechanical behavior of the domain and its constitutive relationships. As the freezing and thawing processes in nature are relatively slow, the state variables are smooth, except for the cryogenic suction, which exhibit a sharp increase (jump) for every degree Celsius below zero. As a consequence, the cryogenic suction is considered here a primary state variable, to have it directly computed from solving the finite element equations, rather than been calculated in the post processing. However, its magnitude is restrained by the Clausius-Clapeyron relation. Accordingly, the model is formulated based on displacement-pressure-enthalpy-cryosuction formulation, with the primary state variables: solid phase displacement $\mathbf{u}$, water mixture pressure p_m, water mixture specific enthalpy h_m, solid specific enthalpy h_s, and cryousuction s_c. The other 16 variables are dependent and defined by their relevant constitutive relationships.

The numerical solution is conducted using a mixed finite element discretization scheme in which state variables exhibiting continuous nature are discretized using the standard Galerkin finite element method (SG) and those exhibiting high gradient are discretized using the extended finite element method (XFEM). The mixed discretization scheme is similar to the well-known mixed finite element method in that it allows using different primary state variables (such as pore pressure and solid displacement) but differs in its discretization approach. In the mixed finite element method all primary state variables are discretized using a single discretization scheme (such as SG) but in the mixed discretization scheme, the primary state variables can be discretized in different ways, depending on their physical nature (Al-Khoury and Sluys 2007; Arzanfudi and Al-Khoury 2017). XFEM is an enhanced finite element scheme based on the partition of unity principles to model discontinuities and high gradient fields, regardless of the finite element mesh. It enables using structured and fixed meshes. In this work, the solid phase displacement $\mathbf{u}$, water mixture pressure p_m, water mixture specific enthalpy h_m, and solid specific enthalpy h_s are discretized using SG, and the cryogenic suction s_c is discretized using XFEM.

3 Governing Equations

The representative elementary volume (REV) averaging theory is utilized to formulate the governing equations (Lewis and Schrefler 1998). For a multiphase system, the averaging theory entails that each phase is assumed occupying the whole volume of REV and is distributed continuously over it, regardless of its detailed heterogeneity. The phases are distinct from each other by their physical properties and velocities, and their mass and volume fractions within REV. The size of REV must be significantly larger than the size of heterogeneity of the matter, but much smaller than the size of the bulk material.

The porous domain is assumed saturated, isotropic and non-isothermal with local thermal equilibrium. It constitutes a solid matrix and water, with the solid matrix exhibiting deformation due to coupling

between water freezing, pore expansion and cryogenic suction, and the water exhibiting thermally-induced phase change from liquid to solid ice and vice versa. The three phases (solid, liquid water and ice) might interact physically with each other and exchange mass, momentum and energy at their contact interfacial areas.

As mentioned in Section 2, the model contains 21 state variables, divided into 5 primary state variables and 16 dependent variables. The partial differential equations describing the conservation of momentum, mass and energy in a multiphase porous medium domain are expressed in terms of the primary state variables ($\mathbf{u}$, p_m, h_m, h_s, s_c), as given below in Sections 3.1-3.3. Section 3.4 describes the relevant constitutive relationships for the 16 dependent variables. These two sets of equations, together with the initial and boundary conditions (Section 3.5) formulate the governing field equations, which are numerically solved in Section 4.

3.1 Momentum balance equation

The averaged macroscopic linear momentum balance equation of a multiphase domain constituting a solid phase, a liquid water phase and an ice phase, and subjected to thermo-hydro-mechanical forces can be expressed in an incremental form as

$$\nabla \cdot \left[\mathbf{D}_T \left(\mathbf{L} \frac{\partial \mathbf{u}}{\partial t} - \frac{1}{3} \mathbf{m} \beta_s \frac{\partial T_s}{\partial t} \right) - \mathbf{m} \alpha \frac{\partial p_s}{\partial t} \right] + \frac{\partial \rho_{eff}}{\partial t} \mathbf{g} = 0 \tag{1}$$

where $\mathbf{u}$ is the displacement vector, T_s is the porous matrix temperature, $\mathbf{D}_T$ is the tangential solid stiffness matrix, β_s is the solid volumetric thermal expansion coefficient, α is Biot's coefficient, $\mathbf{g}$ is the gravitational vector, $\mathbf{m} = [1,1,1,0,0,0]^T$, and ρ_{eff} and p_s are the effective mass density and the pressure exerted by the water phase on the solid phase, defined as

$$\begin{aligned} \rho_{eff} &= (1-\varphi)\rho_s + \varphi S_{ice}\rho_{ice} + \varphi S_{lw}\rho_{lw} \\ p_s &= S_{lw} p_{lw} + S_{ice} p_{ice} \end{aligned} \tag{2}$$

and $\mathbf{L}$ is a differential operator, given by

$$\mathbf{L} = \begin{bmatrix} \partial/\partial x & 0 & 0 & \partial/\partial y & 0 & \partial/\partial z \\ 0 & \partial/\partial y & 0 & \partial/\partial x & \partial/\partial z & 0 \\ 0 & 0 & \partial/\partial z & 0 & \partial/\partial y & \partial/\partial x \end{bmatrix}^T \tag{3}$$

in which φ is the porosity, ρ_s, ρ_{lw} and ρ_{ice} are the mass density of solid, liquid water and ice, respectively, and S_{lw} and S_{ice} are the liquid water and ice saturations.

The dependent variables in Eq. (1) are functions of the primary state variables, such that $T_s = T_s(h_s)$, $p_s = p_s(p_m, h_m, s_c)$, and $\rho_{eff} = \rho_{eff}(p_m, h_m)$, with the subscript m denoting the water mixture (liquid water and ice). Using the chain rule, the derivatives of these dependent variables can then be expressed as

$$\frac{\partial T_s}{\partial t}=\frac{\partial T_s}{\partial h_s}\frac{\partial h_s}{\partial t}=\frac{1}{c_{ps}}\frac{\partial h_s}{\partial t} \tag{4}$$

$$\frac{\partial p_s}{\partial t}=\frac{\partial p_s}{\partial h_m}\frac{\partial h_m}{\partial t}+\frac{\partial p_s}{\partial p_m}\frac{\partial p_m}{\partial t}+\frac{\partial p_s}{\partial s_c}\frac{\partial s_c}{\partial t} \tag{5}$$

$$\frac{\partial \rho_{eff}}{\partial t}=\frac{\partial \rho_{eff}}{\partial h_m}\frac{\partial h_m}{\partial t}+\frac{\partial \rho_{eff}}{\partial p_m}\frac{\partial p_m}{\partial t} \tag{6}$$

where c_{ps} is the specific heat capacity of the solid phase, h_m is the water mixture specific enthalpy, h_s is the solid specific enthalpy, and s_c is the cryosuction.

Substituting Eqs. (4)-(6) into Eq. (1), gives

$$\begin{aligned}&\nabla\cdot\left[\mathbf{D}_s\left(\mathbf{L}\frac{\partial \mathbf{u}}{\partial t}-\frac{1}{3}\mathbf{m}\beta_s\frac{1}{c_{ps}}\frac{\partial h_s}{\partial t}\right)-\mathbf{m}\alpha\left(\frac{\partial p_s}{\partial h_m}\frac{\partial h_m}{\partial t}+\frac{\partial p_s}{\partial p_m}\frac{\partial p_m}{\partial t}+\frac{\partial p_s}{\partial s_c}\frac{\partial s_c}{\partial t}\right)\right]\\&+\left(\frac{\partial \rho_{eff}}{\partial h_m}\frac{\partial h_m}{\partial t}+\frac{\partial \rho_{eff}}{\partial p_m}\frac{\partial p_m}{\partial t}\right)\mathbf{g}=0\end{aligned} \tag{7}$$

By this derivation, the momentum balance equation, Eq. (1), is formulated in terms of the primary state variables $\mathbf{u}$, p_m, h_m, h_s and s_c.

3.2 Mass balance equation

The averaged macroscopic mass balance equations for the solid phase, liquid water phase, ice phase and the mixtures are:

Solid matrix phase

The mass balance equation for the solid phase can be expressed as

$$\frac{(1-\varphi)}{\rho_s}\frac{\partial \rho_s}{\partial t}-\frac{\partial \varphi}{\partial t}+(1-\varphi)\mathbf{m}^T\mathbf{L}\frac{\partial \mathbf{u}}{\partial t}=0 \tag{8}$$

The constitutive relationship for the solid mass density can be described as (Lewis and Schrefler 1998)

$$\frac{1}{\rho_s}\frac{\partial \rho_s}{\partial t}=\frac{1}{1-\varphi}\left[(\alpha-\varphi)\frac{1}{K_s}\frac{\partial p_s}{\partial t}-\beta_s(\alpha-\varphi)\frac{\partial T_s}{\partial t}-(1-\alpha)\mathbf{m}^T\mathbf{L}\frac{\partial \mathbf{u}}{\partial t}\right] \tag{9}$$

in which K_s is the bulk modulus of the solid grains.

Substituting Eqs. (4)-(5) into Eq. (9) gives

$$\begin{aligned}\frac{1}{\rho_s}\frac{\partial \rho_s}{\partial t}=\frac{1}{1-\varphi}\Bigg(&(\alpha-\varphi)\frac{1}{K_s}\left(\frac{\partial p_s}{\partial h_m}\frac{\partial h_m}{\partial t}+\frac{\partial p_s}{\partial p_m}\frac{\partial p_m}{\partial t}+\frac{\partial p_s}{\partial s_c}\frac{\partial s_c}{\partial t}\right)-\\&\beta_s(\alpha-\varphi)\frac{1}{c_{ps}}\frac{\partial h_s}{\partial t}-(1-\alpha)\mathbf{m}^T\mathbf{L}\frac{\partial \mathbf{u}}{\partial t}\Bigg)\end{aligned} \tag{10}$$

Substituting Eq. (10) into Eq. (8) and rearranging, yields

$$\frac{\partial \varphi}{\partial t} = \frac{\alpha - \varphi}{K_s}\left(\frac{\partial p_s}{\partial h_m}\frac{\partial h_m}{\partial t} + \frac{\partial p_s}{\partial p_m}\frac{\partial p_m}{\partial t} + \frac{\partial p_s}{\partial s_c}\frac{\partial s_c}{\partial t}\right) - \beta_s(\alpha - \varphi)\frac{1}{c_{ps}}\frac{\partial h_s}{\partial t} - (\varphi - \alpha)\mathbf{m}^T\mathbf{L}\frac{\partial \mathbf{u}}{\partial t} \tag{11}$$

which indicates that the porosity is a function of enthalpy, pore pressure, cryosuction and solid matrix displacement.

Liquid water phase

The mass balance equation for the liquid water phase can be written as

$$\frac{\partial \varphi}{\partial t} + \frac{\varphi}{\rho_{lw}}\frac{\partial \rho_{lw}}{\partial t} + \frac{\varphi}{S_{lw}}\frac{\partial S_{lw}}{\partial t} + \frac{1}{S_{lw}\rho_{lw}}\nabla\cdot(\rho_{lw}\mathbf{v}_{lw}) + \varphi\mathbf{m}^T\mathbf{L}\frac{\partial \mathbf{u}}{\partial t} = -\frac{\dot{m}_{lw\to ice}}{S_{lw}\rho_{lw}} \tag{12}$$

in which $\mathbf{v}_{lw}$ is the mass averaged velocity of liquid water, and $\dot{m}_{lw\to ice}$ is the mass exchange rate between liquid water and ice, arising from the phase change.

Inserting Eq. (11) into Eq. (12), yields

$$\begin{aligned}&\frac{\alpha - \varphi}{K_s}\left(\frac{\partial p_s}{\partial h_m}\frac{\partial h_m}{\partial t} + \frac{\partial p_s}{\partial p_m}\frac{\partial p_m}{\partial t} + \frac{\partial p_s}{\partial s_c}\frac{\partial s_c}{\partial t}\right) - \beta_s(\alpha - \varphi)\frac{1}{c_{ps}}\frac{\partial h_s}{\partial t}\\ &+ \alpha\mathbf{m}^T\mathbf{L}\frac{\partial \mathbf{u}}{\partial t} + \frac{\varphi}{\rho_{lw}}\frac{\partial \rho_{lw}}{\partial t} + \frac{\varphi}{S_{lw}}\frac{\partial S_{lw}}{\partial t} + \frac{1}{S_{lw}\rho_{lw}}\nabla\cdot(\rho_{lw}\mathbf{v}_{lw}) = -\frac{\dot{m}_{lw\to ice}}{S_{lw}\rho_{lw}}\end{aligned} \tag{13}$$

Applying the chain rule to the liquid water density and saturation, gives

$$\frac{\partial \rho_{lw}}{\partial t} = \frac{\partial \rho_{lw}}{\partial p_m}\frac{\partial p_m}{\partial t} + \frac{\partial \rho_{lw}}{\partial h_m}\frac{\partial h_m}{\partial t} \tag{14}$$

$$\frac{\partial S_{lw}}{\partial t} = \frac{\partial S_{lw}}{\partial p_m}\frac{\partial p_m}{\partial t} + \frac{\partial S_{lw}}{\partial h_m}\frac{\partial h_m}{\partial t} \tag{15}$$

Substituting Eqs. (14)-(15) into Eq. (13), and re-arranging, results in

$$\begin{aligned}&\left(\frac{\alpha - \varphi}{K_s}S_{lw}\rho_{lw}\frac{\partial p_s}{\partial p_m} + \varphi S_{lw}\frac{\partial \rho_{lw}}{\partial p_m} + \varphi\rho_{lw}\frac{\partial S_{lw}}{\partial p_m}\right)\frac{\partial p_m}{\partial t}\\ &+ \left(\frac{\alpha - \varphi}{K_s}S_{lw}\rho_{lw}\frac{\partial p_s}{\partial h_m} + \varphi S_{lw}\frac{\partial \rho_{lw}}{\partial h_m} + \varphi\rho_{lw}\frac{\partial S_{lw}}{\partial h_m}\right)\frac{\partial h_m}{\partial t}\\ &+ \frac{\alpha - \varphi}{K_s}S_{lw}\rho_{lw}\frac{\partial p_s}{\partial s_c}\frac{\partial s_c}{\partial t} - \beta_s(\alpha - \varphi)S_{lw}\rho_{lw}\frac{1}{c_{ps}}\frac{\partial h_s}{\partial t} + \alpha S_{lw}\rho_{lw}\mathbf{m}^T\mathbf{L}\frac{\partial \mathbf{u}}{\partial t}\\ &+ \nabla\cdot(\rho_{lw}\mathbf{v}_{lw}) = -\dot{m}_{lw\to ice}\end{aligned} \tag{16}$$

Ice phase

Similar to liquid water, the mass balance equation of the ice phase can readily be derived to give

$$
\begin{aligned}
&\left(\frac{\alpha-\varphi}{K_s}S_{ice}\rho_{ice}\frac{\partial p_s}{\partial p_m}+\varphi S_{ice}\frac{\partial \rho_{ice}}{\partial p_m}+\varphi\rho_{ice}\frac{\partial S_{ice}}{\partial p_m}\right)\frac{\partial p_m}{\partial t}+\\
&+\left(\frac{\alpha-\varphi}{K_s}S_{ice}\rho_{ice}\frac{\partial p_s}{\partial h_m}+\varphi S_{ice}\frac{\partial \rho_{ice}}{\partial h_m}+\varphi\rho_{ice}\frac{\partial S_{ice}}{\partial h_m}\right)\frac{\partial h_m}{\partial t}\\
&+\frac{\alpha-\varphi}{K_s}S_{ice}\rho_{ice}\frac{\partial p_s}{\partial s_c}\frac{\partial s_c}{\partial t}-\beta_s(\alpha-\varphi)S_{ice}\rho_{ice}\frac{1}{c_{ps}}\frac{\partial h_s}{\partial t}+\alpha S_{ice}\rho_{ice}\mathbf{m}^T\mathbf{L}\frac{\partial \mathbf{u}}{\partial t}\\
&+\nabla\cdot(\rho_{ice}\mathbf{v}_{ice})=\dot{m}_{lw\to ice}
\end{aligned}
\tag{17}
$$

where $\mathbf{v}_{ice}$ is the mass averaged velocity of ice.

Water mixture (liquid water and ice)

Consider the following identities:

$$
\begin{aligned}
&S_{lw}+S_{ice}=1\\
&\rho_m=S_{lw}\rho_{lw}+S_{ice}\rho_{ice}\\
&S_{lw}\frac{\partial \rho_{lw}}{\partial h_m}+\rho_{lw}\frac{\partial S_{lw}}{\partial h_m}+S_{ice}\frac{\partial \rho_{ice}}{\partial h_m}+\rho_{ice}\frac{\partial S_{ice}}{\partial h_m}\\
&=\frac{\partial(S_{lw}\rho_{lw})}{\partial h_m}+\frac{\partial(S_{ice}\rho_{ice})}{\partial h_m}\\
&=\frac{\partial(S_{lw}\rho_{lw}+S_{ice}\rho_{ice})}{\partial h_m}\\
&=\frac{\partial \rho_m}{\partial h_m}
\end{aligned}
\tag{18}
$$

Summing Eqs. (16) and (17), and using Eq. (18) gives the mass balance equation of the water mixture, as

$$
\begin{aligned}
&\left(\frac{\alpha-\varphi}{K_s}\rho_m\frac{\partial p_s}{\partial p_m}+\varphi\frac{\partial \rho_m}{\partial p_m}\right)\frac{\partial p_m}{\partial t}+\left(\frac{\alpha-\varphi}{K_s}\rho_m\frac{\partial p_s}{\partial h_m}+\varphi\frac{\partial \rho_m}{\partial h_m}\right)\frac{\partial h_m}{\partial t}\\
&+\frac{\alpha-\varphi}{K_s}\rho_m\frac{\partial p_s}{\partial s_c}\frac{\partial s_c}{\partial t}-\beta_s(\alpha-\varphi)\rho_m\frac{1}{c_{ps}}\frac{\partial h_s}{\partial t}+\alpha\rho_m\mathbf{m}^T\mathbf{L}\frac{\partial \mathbf{u}}{\partial t}\\
&+\nabla\cdot(\rho_{lw}\mathbf{v}_{lw}+\rho_{ice}\mathbf{v}_{ice})=0
\end{aligned}
\tag{19}
$$

The ice velocity is negligible and can be ignored ($\mathbf{v}_{ice}=0$), and the liquid water velocity can be described using Darcy's law, as

$$
\mathbf{v}_{lw}=\frac{\mathbf{k}k_{rlw}}{\mu_{lw}}\left(-\nabla p_{lw}+\rho_{lw}\mathbf{g}\right)
\tag{20}
$$

in which k_{rlw} and μ_{lw} are the relative permeability and dynamic viscosity of the liquid water.

The water mixture pressure p_m in Eq. (19) can be expressed as

$$
p_m=p_{lw}+s_c
\tag{21}
$$

which indicates that before freezing, $s_c = 0$, and hence, the mixture pressure is equal to the liquid pressure p_{lw}; but upon freezing, the cryogenic suction builds up and rapidly becomes much higher than the liquid pressure, leading to the mixture pressure to be nearly equal to the ice pressure p_{ice}.

Inserting Eq. (21) into Eq. (20), gives

$$\mathbf{v}_{lw} = \frac{\mathbf{k}k_{rlw}}{\mu_{lw}}\left(-\nabla p_m + \nabla s_c + \rho_{lw}\mathbf{g}\right) \tag{22}$$

Substituting Eq. (22) into Eq. (19) results in

$$d_1\frac{\partial p_m}{\partial t} + d_2\frac{\partial h_m}{\partial t} + d_3\frac{\partial h_s}{\partial t} + d_4\mathbf{m}^T\mathbf{L}\frac{\partial \mathbf{u}}{\partial t} + e_1\frac{\partial s_c}{\partial t} + \nabla\cdot\left(-\mathbf{c}_1\nabla p_m - \mathbf{c}_2\nabla s_c + \mathbf{G}_1\right) = 0 \tag{23}$$

in which

$$\begin{aligned}
d_1 &= \varphi\frac{\partial \rho_m}{\partial p_m} + \frac{\alpha-\varphi}{K_s}\rho_m\frac{\partial p_s}{\partial p_m} & d_4 &= \alpha\rho_m \\
d_2 &= \varphi\frac{\partial \rho_m}{\partial h_m} + \frac{\alpha-\varphi}{K_s}\rho_m\frac{\partial p_s}{\partial h_m} & \mathbf{c}_1 &= \rho_{lw}\frac{\mathbf{k}k_{rlw}}{\mu_{lw}} \\
d_3 &= -\rho_m\beta_s(\alpha-\varphi)\frac{1}{c_{ps}} & \mathbf{c}_2 &= -\rho_{lw}\frac{\mathbf{k}k_{rlw}}{\mu_{lw}} \\
e_1 &= \frac{\alpha-\varphi}{K_s}\rho_m\frac{\partial p_s}{\partial s_c} & \mathbf{G}_1 &= \rho_{lw}\frac{\mathbf{k}k_{rlw}}{\mu_{lw}}\rho_{lw}\mathbf{g}
\end{aligned} \tag{24}$$

As for the momentum balance equation, the mass balance equation, Eq. (23), is formulated in terms of the primary state variables.

3.3 Energy balance equation

The averaged macroscopic energy balance equation for a multiphase domain exhibiting local thermal equilibrium can be expressed as

$$\begin{aligned}
&\frac{\partial}{\partial t}\left[(1-\varphi)\rho_s h_s + \varphi\rho_m h_m - (1-\varphi)p_s' - \varphi p_m\right] \\
&\qquad + \varphi\rho_m h_m\mathbf{m}^T\mathbf{L}\frac{\partial \mathbf{u}}{\partial t} + \nabla\cdot\left(\rho_{lw}h_{lw}\mathbf{v}_{lw}\right) + \nabla\cdot\left(-\boldsymbol{\lambda}_{eff}\cdot\nabla T_s\right) = 0
\end{aligned} \tag{25}$$

where h_{lw} is the specific enthalpy of liquid water, p_s' is the mean effective stress, and

$$\boldsymbol{\lambda}_{eff} = (1-\varphi)\boldsymbol{\lambda}_s + \varphi S_{ice}\boldsymbol{\lambda}_{ice} + \varphi S_{lw}\boldsymbol{\lambda}_{lw} \tag{26}$$

is the effective thermal conductivity of the porous domain, with λ_s, λ_{lw} and λ_{ice} denoting the thermal conductivity of the porous solid, liquid water and ice, respectively.

The temperature gradient can be described as

$$\nabla T_s = \left(\frac{\partial T}{\partial h}\right)_s \nabla h_s = \frac{1}{c_{ps}}\nabla h_s \tag{27}$$

Substituting Eqs. (20) and (27) into Eq. (25), and expanding the time derivatives, results in

$$\begin{aligned}&\left(\rho_m h_m-\rho_s h_s-p_m+p_s'\right)\frac{\partial\varphi}{\partial t}+\left(1-\varphi\right)h_s\frac{\partial\rho_s}{\partial t}+\left(1-\varphi\right)\rho_s\frac{\partial h_s}{\partial t}+\varphi\rho_m\frac{\partial h_m}{\partial t}+\varphi h_m\frac{\partial\rho_m}{\partial t}\\&-\left(1-\varphi\right)\frac{\partial p_s'}{\partial t}-\varphi\frac{\partial p_m}{\partial t}+\varphi\rho_m h_m\mathbf{m}^T\mathbf{L}\frac{\partial\mathbf{u}}{\partial t}+\nabla\cdot\left[\rho_{lw}h_{lw}\frac{\mathbf{k}k_{rlw}}{\mu_{lw}}\left(-\nabla p_m+\nabla s_c+\rho_{lw}\mathbf{g}\right)\right]\\&+\nabla\cdot\left(-\boldsymbol{\lambda}_{eff}\cdot\frac{1}{c_{ps}}\nabla h_s\right)=0\end{aligned}\tag{28}$$

Applying the chain rule to the mixture mass density time derivative, gives

$$\frac{\partial\rho_m}{\partial t}=\frac{\partial\rho_m}{\partial p_m}\frac{\partial p_m}{\partial t}+\frac{\partial\rho_m}{\partial h_m}\frac{\partial h_m}{\partial t}\tag{29}$$

Substituting Eq. (10), Eq. (11) and Eq. (29) into (28) leads to

$$d_5\frac{\partial h_s}{\partial t}+d_6\frac{\partial h_m}{\partial t}+d_7\frac{\partial p_m}{\partial t}+d_8\mathbf{m}^T\mathbf{L}\frac{\partial\mathbf{u}}{\partial t}+e_2\frac{\partial s_c}{\partial t}+\nabla\cdot\left[-\mathbf{c}_3\nabla p_m-\mathbf{c}_4\nabla s_c-\mathbf{c}_5\nabla h_s+\mathbf{G}_2\right]=0\tag{30}$$

in which

$$\begin{aligned}d_5&=\left(1-\varphi\right)\rho_s-\beta_s\left(\alpha-\varphi\right)\left(\rho_m h_m-p_m+p_s'\right)\frac{1}{c_{ps}}\\d_6&=\varphi\rho_m+\varphi h_m\frac{\partial\rho_m}{\partial h_m}+\left(\rho_m h_m-p_m+p_s'\right)\frac{\alpha-\varphi}{K_s}\frac{\partial p_s}{\partial h_m}\\d_7&=\left(\rho_m h_m-p_m+p_s'\right)\frac{\alpha-\varphi}{K_s}\frac{\partial p_s}{\partial p_m}-\varphi+\varphi h_m\frac{\partial\rho_m}{\partial p_m}\\d_8&=-\left[\begin{array}{l}\left(1-\varphi\right)\rho_s h_s-\alpha\rho_m h_m\\\quad+\left(\varphi-\alpha\right)\left(-p_m+p_s'\right)-\left(1-\varphi\right)K_T\end{array}\right]\\e_2&=\left(\rho_m h_m-p_m+p_s'\right)\frac{\alpha-\varphi}{K_s}\left(\frac{\partial p_s}{\partial s_c}\right)\end{aligned}\qquad\begin{aligned}\mathbf{c}_3&=\rho_{lw}h_{lw}\frac{\mathbf{k}k_{rlw}}{\mu_{lw}}\\\mathbf{c}_4&=-\rho_{lw}h_{lw}\frac{\mathbf{k}k_{rlw}}{\mu_{lw}}\\\mathbf{c}_5&=\frac{1}{c_{ps}}\boldsymbol{\lambda}_{eff}\\\mathbf{G}_2&=\rho_{lw}h_{lw}\frac{\mathbf{k}k_{rlw}}{\mu_{lw}}\rho_{lw}\mathbf{g}\end{aligned}\tag{31}$$

in which K_T is the bulk modulus of the solid skeleton. Eq. (30) is the energy balance equation formulated in terms of the primary state variables.

Since the specific enthalpies of water and solid phases are primary state variables, the local thermal equilibrium can only be satisfied by imposing this constraint:

$$T_s-T_m=0\tag{32}$$

in which T_m is the water mixture temperature. Using Eq. (27), this equation can be written as

$$\frac{1}{c_{ps}}h_s-T_m=0\tag{33}$$

3.4 Constitutive relationships

3.4.1 Porous matrix

The stiffness matrix of a three-dimensional, isotropic solid is described as

$$\mathbf{D}_T = \frac{E_T(T)}{(1+\nu_s)(1-2\nu_s)} \begin{bmatrix} 1-\nu_s & \nu_s & \nu_s & 0 & 0 & 0 \\ & 1-\nu_s & \nu_s & 0 & 0 & 0 \\ & & 1-\nu_s & 0 & 0 & 0 \\ & & & \frac{1-2\nu_s}{2} & 0 & 0 \\ & \textit{Symmetric} & & & \frac{1-2\nu_s}{2} & 0 \\ & & & & & \frac{1-2\nu_s}{2} \end{bmatrix} \tag{34}$$

where ν_s is Poisson's ratio, and $E_T(T)$ is a temperature-dependent elastic modulus, defined, here, as

$$E_T(T) = E_0 e^{-b(T_s - T_0)} \tag{35}$$

where E_0 is the Young's modulus at a reference temperature T_0, and b is a material parameter.

It is worth noting, though, that the assumption of a temperature-dependent linear elastic behavior of the solid matrix might be reasonable during freezing, but upon thawing and repetitive freezing-thawing cycles, the behavior might become non-linear elasto-plastic. Modeling such a behavior will be treated in a follow up work.

3.4.2 Water equation of state (EOS)

The thermodynamic state variables and properties of the liquid water, ice and the water mixture, ρ_m, T_m, ρ_{ice}, ρ_{lw}, S_{ice}, S_{lw}, λ_{ice}, λ_{lw}, μ_{lw} are obtained from the equation of state of water, adopted from IAPWS (2007) and other relevant literature, given in Appendix A.

3.4.3 Melting point depression

Pore liquids in porous media freeze at temperatures well below their bulk freezing (melting) points. The melting point is inversely proportional to the pore size, as given by the Gibbs–Thomson equation. The use of this equation for porous media requires knowledge of the pore geometry, solid-liquid interface energy and the wetting angle inside the pores; quantities which are normally difficult to measure, especially for geoscience applications. Instead, several empirical relationships have been obtained from experimental measurements of macroscopic specimens, or from assuming the similarity between the soil water curves (SWC), describing the relationship between the capillary pressure and the moisture content, and the soil freezing curves (SFC), describing the relationship between the sub-zero temperatures and the unfrozen water content. Kurylyk and Watanabe (2013) presented an interesting review describing different forms of the Clapeyron equation and empirical methods for describing the SFC relationships. Here, we adopt an exponential function of the form:

$$S_{lw} = S^* + \left(1 - S^*\right) e^{a\left(T_w - T_f\right)} \tag{36}$$

in which S^* is the residual unfrozen water content at a relatively cold condition, T_f is the bulk freezing temperature, and a is a material constant. This kind of constitutive relationships are easy to implement and can readily be obtained from relatively simple laboratory experiments on the type of soil under study. Nevertheless, the proposed model is generic and any other constitutive relationship can be considered.

3.4.4 Cryogenic suction

As indicated in Section 2, the cryogenic suction, s_c, exhibits a jump at every degree Celsius below zero. As a consequence, the cryogenic suction is considered here a primary state variable, to have it directly computed from solving the finite element equations (see Eq. (69)), rather than been calculated in the post processing. However, the computed quantity has to satisfy the Clausius-Clapeyron relation (Lewis and Schrefler 1998):

$$s_c = -\rho_{ice} L_f \ln \frac{T_m}{T_f} \tag{37}$$

where L_f is the latent heat of fusion of water. To satisfy this condition, the following constraint is imposed:

$$-\rho_{ice} L_f \ln \frac{T_m}{T_f} - s_c = 0 \tag{38}$$

which, for simplicity of notation, can be written as

$$f_{sc} - s_c = 0 \tag{39}$$

3.4.5 Relative permeability

Even though the domain is fully saturated, the water exhibits phase change during freezing and thawing, giving rise to a quasi-partially saturated condition within the water phase. As for the partially saturated conditions, calculating this effect necessitates the use of the relative permeability coefficient, as given in Eq. (20). Here, the relative permeability of liquid water is described based on the Brooks and Corey relationship (Brooks and Corey 1964):

$$k_{rlw} = S_{lw}^{(2+3\eta)/\eta} \tag{40}$$

where η is a material constant.

3.5 Initial and boundary conditions

Initially, at $t = 0$, the primary state variables are expressed as

$$g(\mathbf{x}, 0) = g_0(\mathbf{x}) \tag{41}$$

where g can be any of the primary state variables $\mathbf{u}$, p_m, h_m, h_s, or s_c.

The Dirichlet boundary conditions might be described as

$$j(t) = \hat{j}(t) \quad \text{on } \Gamma_u \tag{42}$$

where Γ_u is the Dirichlet boundary and j can be any of the primary state variables.

The Neumann boundary conditions for the mechanical, hydraulic and conductive and convective thermal boundary conditions might be described, respectively, as

$$\begin{aligned} &\hat{\mathbf{t}} = \boldsymbol{\sigma} \cdot \mathbf{n} \\ &\hat{q}_{lw} = \rho_{lw} \mathbf{v}_{lw} \cdot \mathbf{n} \\ &\hat{Q}_{\text{cond}} = -\lambda_{eff} \nabla T_s \cdot \mathbf{n} \\ &\hat{Q}_{\text{conv}} = \rho_{lw} h_{lw} \mathbf{v}_{lw} \cdot \mathbf{n} \end{aligned} \qquad \text{on} \quad \Gamma_q \tag{43}$$

where Γ_q is the Neumann boundary; $\hat{\mathbf{t}}$ is the prescribed traction; $\hat{q}_{lw}$ is the prescribed mass flow rate of liquid water; and $\hat{Q}_{\text{cond}}$ and $\hat{Q}_{\text{conv}}$ are the prescribed conductive and convective heat fluxes, respectively.

4 Finite element mixed discretization

The model encompasses state variables of significantly different nature, describing highly coupled thermo-hydro-mechanical processes. It comprises porous matrix deformation and heat and fluid flow occurring due to gravity, buoyancy, thermal expansion and cryogenic suction. Discretizing such a system using standard finite element method can cause spurious oscillations and requires extensive CPU time and capacity. Importantly, the standard finite element method fails to capture the jump in the cryogenic suction, as it will be highlighted in the numerical example in Section 6.

Here, a mixed finite element discretization scheme is utilized for modeling relatively high freezing-thawing rates in porous media. The primary state variables that represent relatively smooth, continuous fields, namely the displacement, enthalpy and pressure, are discretized using the standard finite element method, and the cryogenic suction is discretized using the partition of unity method within the framework of the extended finite element method. A fixed and structured finite element discretization scheme is adopted.

4.1 Weak form formulation

The weighted residual method is utilized to formulate the finite element equations. In total, five equations are discretized: three conservation equations: momentum (Eqs.(7)), mass (Eq. (23)) and energy (Eq. (30)); a local thermal equilibrium constraint equation (Eq. (33)); and a cryosuction constraint equation (Eq. (39)).

Appling the standard weighted residual discretization procedure to Eqs. (7), (23), (30), and (33) yields:

Momentum balance:

$$
\begin{aligned}
&-\int_\Omega \mathbf{L}^T w\mathbf{D}_s\mathbf{L}\frac{\partial \mathbf{u}}{\partial t}d\Omega+\int_\Omega \mathbf{L}^T w\mathbf{D}_s\frac{1}{3}\mathbf{m}\beta_s\frac{1}{c_{ps}}\frac{\partial h_s}{\partial t}d\Omega+\int_\Omega \mathbf{L}^T w\mathbf{m}\alpha\frac{\partial p_s}{\partial h_m}\frac{\partial h_m}{\partial t}d\Omega\\
&+\int_\Omega \mathbf{L}^T w\mathbf{m}\alpha\frac{\partial p_s}{\partial p_m}\frac{\partial p_m}{\partial t}d\Omega+\int_\Omega \mathbf{L}^T w\mathbf{m}\alpha\frac{\partial p_s}{\partial s_c}\frac{\partial s_c}{\partial t}d\Omega\\
&+\int_\Omega w\frac{\partial \rho_{eff}}{\partial h_m}\frac{\partial h_m}{\partial t}\mathbf{g}d\Omega+\int_\Omega w\frac{\partial \rho_{eff}}{\partial p_m}\frac{\partial p_m}{\partial t}\mathbf{g}d\Omega+\int_{\Gamma_q} w\frac{\partial \hat{\mathbf{t}}}{\partial t}d\Gamma=0
\end{aligned}
\tag{44}
$$

Mass balance:

$$
\begin{aligned}
&\int_\Omega wd_1\frac{\partial p_m}{\partial t}d\Omega+\int_\Omega wd_2\frac{\partial h_m}{\partial t}d\Omega+\int_\Omega wd_3\frac{\partial h_s}{\partial t}d\Omega+\int_\Omega wd_4\mathbf{m}^T\mathbf{L}\frac{\partial \mathbf{u}}{\partial t}d\Omega+\int_\Omega we_1\frac{\partial s_c}{\partial t}d\Omega\\
&-\int_\Omega \nabla w\cdot\left(-\mathbf{c}_1\nabla p_m-\mathbf{c}_2\nabla s_c+\mathbf{G}_1\right)d\Omega+\int_{\Gamma_q} w\hat{q}_{lw}d\Gamma=0
\end{aligned}
\tag{45}
$$

Energy balance:

$$
\begin{aligned}
&\int_\Omega wd_5\frac{\partial h_s}{\partial t}d\Omega+\int_\Omega wd_6\frac{\partial h_m}{\partial t}d\Omega+\int_\Omega wd_7\frac{\partial p_m}{\partial t}d\Omega+\int_\Omega wd_8\mathbf{m}^T\mathbf{L}\frac{\partial \mathbf{u}}{\partial t}d\Omega+\int_\Omega we_2\frac{\partial s_c}{\partial t}d\Omega\\
&-\int_\Omega \nabla w\cdot\left(-\mathbf{c}_3\nabla p_m-\mathbf{c}_4\nabla s_c-\mathbf{c}_5\nabla h_s+\mathbf{G}_2\right)d\Omega+\int_{\Gamma_q} w\hat{Q}_{\text{adv}}d\Gamma+\int_{\Gamma_q} w\hat{Q}_{\text{cond}}d\Gamma=0
\end{aligned}
\tag{46}
$$

Local thermal equilibrium constraint:

$$
\int_\Omega w\frac{1}{c_{ps}}h_s d\Omega-\int_\Omega wT_m d\Omega=0 \tag{47}
$$

Appling the partition of unity weighted residual discretization procedure to the cryosuction constraint equation, Eq. (39), yields

Cryosuction constraint:

Continuous:

$$
\int_\Omega wf_{sc}d\Omega-\int_\Omega ws_c d\Omega=0 \tag{48}
$$

Enhanced:

$$
\int_\Omega w^* f_{sc}d\Omega-\int_\Omega w^* s_c d\Omega=0 \tag{49}
$$

where w and w^* are the standard and enhanced weighting functions.

4.2 Linearization

The Newton-Raphson method is utilized to linearize the problem. The primary state variables and their time derivatives and gradients are linearized as

$$
\begin{aligned}
y^{r+1} &= y^r + \delta y \\
\dot{y}^{r+1} &= \dot{y}^r + \delta \dot{y} \quad ; \quad y \equiv \mathbf{u}, p_m, h_m, h_s, s_c \\
\nabla y^{r+1} &= \nabla y^r + \delta \nabla y
\end{aligned} \tag{50}
$$

where $r+1$ denotes the current iteration, and δ is the associated variation in the variable.

The dependent variables; $T_m = T_m(p_m, h_m)$, $\rho_{eff} = \rho_{eff}(p_m, h_m)$, $f_{sc} = f_{sc}(p_m, h_m)$ and $p_s = p_s(p_m, h_m, s_c)$, and their derivatives are linearized as

$$
x^{r+1} = x^r + \left(\frac{\partial x}{\partial h_m}\right)^r \delta h_m + \left(\frac{\partial x}{\partial p_m}\right)^r \delta p_m \quad ; \quad x \equiv T_m, \rho_{eff}, f_{sc} \tag{51}
$$

$$
\left(\frac{\partial \rho_{eff}}{\partial h_m}\right)^{r+1} = \left(\frac{\partial \rho_{eff}}{\partial h_m}\right)^r + \left(\frac{\partial^2 \rho_{eff}}{\partial {h_m}^2}\right)^r \delta h_m + \left(\frac{\partial^2 \rho_{eff}}{\partial h_m \partial p_m}\right)^r \delta p_m \tag{52}
$$

$$
\left(\frac{\partial \rho_{eff}}{\partial p_m}\right)^{r+1} = \left(\frac{\partial \rho_{eff}}{\partial p_m}\right)^r + \left(\frac{\partial^2 \rho_{eff}}{\partial p_m \partial h_m}\right)^r \delta h_m + \left(\frac{\partial^2 \rho_{eff}}{\partial {p_m}^2}\right)^r \delta p_m \tag{53}
$$

$$
{p_s}^{r+1} = {p_s}^r + \left(\frac{\partial p_s}{\partial h_m}\right)^r \delta h_m + \left(\frac{\partial p_s}{\partial p_m}\right)^r \delta p_m + \left(\frac{\partial p_s}{\partial s_c}\right)^r \delta s_c \tag{54}
$$

$$
\left(\frac{\partial p_s}{\partial h_m}\right)^{r+1} = \left(\frac{\partial p_s}{\partial h_m}\right)^r + \left(\frac{\partial^2 p_s}{\partial {h_m}^2}\right)^r \delta h_m + \left(\frac{\partial^2 p_s}{\partial h_m \partial p_m}\right)^r \delta p_m + \left(\frac{\partial^2 p_s}{\partial h_m \partial s_c}\right)^r \delta s_c \tag{55}
$$

$$
\left(\frac{\partial p_s}{\partial p_m}\right)^{r+1} = \left(\frac{\partial p_s}{\partial p_m}\right)^r + \left(\frac{\partial^2 p_s}{\partial p_m \partial h_m}\right)^r \delta h_m + \left(\frac{\partial^2 p_s}{\partial {p_m}^2}\right)^r \delta p_m + \left(\frac{\partial^2 p_s}{\partial p_m \partial s_c}\right)^r \delta s_c \tag{56}
$$

$$
\left(\frac{\partial p_s}{\partial s_c}\right)^{r+1} = \left(\frac{\partial p_s}{\partial s_c}\right)^r + \left(\frac{\partial^2 p_s}{\partial s_c \partial h_m}\right)^r \delta h_m + \left(\frac{\partial^2 p_s}{\partial s_c \partial p_m}\right)^r \delta p_m + \left(\frac{\partial^2 p_s}{\partial {s_c}^2}\right)^r \delta s_c \tag{57}
$$

The coefficients in Eqs. (23) and (30) $d_1, d_2, d_6, d_7, d_8, e_1, e_2 \equiv g(p_m, h_m, s_c)$, and $d_3, d_4, d_5, \mathbf{c}_1, \mathbf{c}_2, \mathbf{c}_3, \mathbf{c}_4, \mathbf{c}_5, \mathbf{G}_1, \mathbf{G}_2 \equiv j(p_m, h_m)$ are linearized as

$$
g^{r+1} = g^r + \left(\frac{\partial g}{\partial h_m}\right)^r \delta h_m + \left(\frac{\partial g}{\partial p_m}\right)^r \delta p_m + \left(\frac{\partial g}{\partial s_c}\right)^r \delta s_c \quad ; \quad g \equiv d_1, d_2, d_6, d_7, d_8, e_1, e_2 \tag{58}
$$

$$
j^{r+1} = j^r + \left(\frac{\partial j}{\partial h_m}\right)^r \delta h_m + \left(\frac{\partial j}{\partial p_m}\right)^r \delta p_m \quad ; \quad j \equiv d_3, d_4, d_5, \mathbf{c}_1, \mathbf{c}_2, \mathbf{c}_3, \mathbf{c}_4, \mathbf{c}_5, \mathbf{G}_1, \mathbf{G}_2 \tag{59}
$$

The evolution of porosity, Eq. (11), and the temperature-dependent elastic modulus, Eq. (35), are treated explicitly by updating their values at every time step.

Substituting Eqs. (50)-(59) into Eqs. (45)-(47), eliminating the high order differentials, and rearranging, yields the linearized weak form finite element equations for the mass balance, energy balance, local thermal equilibrium constraint, and the cryosuction constraint. These equations are listed in Appendix B.

4.3 Mixed FE formulation

Using the Galerkin finite element method, the solid displacement, mixture pressure, mixture specific enthalpy, and solid phase specific enthalpy are discretized as

$$\mathbf{u}(\mathbf{x},t) = \mathbf{N}_u(\mathbf{x})\bar{\mathbf{u}}(t) \tag{60}$$

$$p_m(\mathbf{x},t) = \mathbf{N}(\mathbf{x})\bar{\mathbf{p}}_m(t) \tag{61}$$

$$h_m(\mathbf{x},t) = \mathbf{N}(\mathbf{x})\bar{\mathbf{h}}_m(t) \tag{62}$$

$$h_s(\mathbf{x},t) = \mathbf{N}(\mathbf{x})\bar{\mathbf{h}}_s(t) \tag{63}$$

Using the partition of unity, the cryogenic suction is discretized as

$$s_c(\mathbf{x},t) = \mathbf{N}(\mathbf{x})\bar{\mathbf{s}}_c(t) + \mathbf{N}^*(\mathbf{x})\tilde{\mathbf{s}}_c(t) \tag{64}$$

in which the barred values are the nodal values, **N** is the standard finite element shape function vector, and

$$\mathbf{N}^*(\mathbf{x}) = \mathbf{N}(\mathbf{x})\psi(\mathbf{x}) \tag{65}$$

is the enhanced shape function, with ψ the partition of unity enhancement function, described here as

$$\psi(\mathbf{x}) = e^{-\frac{\|\mathbf{x}-\mathbf{x}^*\|}{\ell_c}} \tag{66}$$

in which $\mathbf{x}^*$ is the normal projection of **x** on the freezing boundary Γ_q, and ℓ_c is a characteristic length, which can be a property of the porous matrix.

The weight functions in Eqs. (44)-(49) are defined as

$$w = \mathbf{N} \tag{67}$$

$$w^* = \mathbf{N}^* \tag{68}$$

Substituting Eqs. (60)-(68) into the linearized equations in Appendix B gives the finite element equations, which can be described in a compact form as

$$\mathbf{K}\,\delta\mathbf{X} + \mathbf{C}\,\delta\dot{\mathbf{X}} = \mathbf{f} - \mathbf{K}_0\mathbf{X}^r - \mathbf{C}_0\dot{\mathbf{X}}^r \tag{69}$$

where

$$\delta\mathbf{X} = \left(\delta\bar{\mathbf{u}} \quad \delta\bar{\mathbf{p}}_m \quad \delta\bar{\mathbf{h}}_m \quad \delta\bar{\mathbf{h}}_s \quad \delta\bar{\mathbf{s}}_c \quad \delta\tilde{\mathbf{s}}_c\right)^T$$
$$\delta\dot{\mathbf{X}} = \left(\delta\dot{\bar{\mathbf{u}}} \quad \delta\dot{\bar{\mathbf{p}}}_m \quad \delta\dot{\bar{\mathbf{h}}}_m \quad \delta\dot{\bar{\mathbf{h}}}_s \quad \delta\dot{\bar{\mathbf{s}}}_c \quad \delta\dot{\tilde{\mathbf{s}}}_c\right)^T$$
$$\mathbf{X}^r = \left(\bar{\mathbf{u}}^r \quad \bar{\mathbf{p}}_m^r \quad \bar{\mathbf{h}}_m^r \quad \bar{\mathbf{h}}_s^r \quad \bar{\mathbf{s}}_c^r \quad \tilde{\mathbf{s}}_c^r\right) \tag{70}$$
$$\dot{\mathbf{X}}^r = \left(\dot{\bar{\mathbf{u}}}^r \quad \dot{\bar{\mathbf{p}}}_m^r \quad \dot{\bar{\mathbf{h}}}_m^r \quad \dot{\bar{\mathbf{h}}}_s^r \quad \dot{\bar{\mathbf{s}}}_c^r \quad \dot{\tilde{\mathbf{s}}}_c^r\right)^T$$
$$\mathbf{f} = \left(\mathbf{f}_1 \quad \mathbf{f}_2 \quad \mathbf{f}_3 \quad \mathbf{f}_4 \quad \mathbf{f}_5 \quad \mathbf{f}_6\right)^T$$

The coefficients of the matrices and vectors of Eq. (69) are given in Appendix C.

Eq. (69) is a semi-discrete system of equations which can be solved using any of the time integration schemes. Here, we use a fully implicit finite difference time integration scheme.

5 Model verification

Verifying the accuracy of the model against experimental work or numerical codes is not readily accessible, as either the experimental set-ups are not necessarily designed to examine all features of the model, or the numerical codes are not appropriately verified, validated or designed to be utilized as a reference case. Nevertheless, recently, an important comparison exercise is devised to numerically validate the accuracy and performance of TH numerical codes, introduced by Grenier et al. (2018). Thirteen numerical codes with different numerical approaches, spatial and temporal discretization schemes and computational efficiency were tested to examine two-dimensional (2D) thawing benchmark cases.

Here we make use of this exercise to partially verify the introduced THM model. A thawing benchmark case, termed TH2 in Grenier et al. (2018) is simulated. This benchmark case examines heat and fluid flow in a 2D porous medium domain, 3 m x 1 m, initially at 5 °C, and includes a 0.333 m x 0.333 m initially frozen zone at -5°C. The domain is closed at the top and bottom boundaries and insulated against conduction from the top, bottom and right boundaries, but subjected to a head difference of 0.03 m/m from the left boundary. Fig. 1 shows the geometry and initial and boundary conditions of this benchmark case. The analysis is conducted by letting the frozen zone to thaw naturally for approximately 55 hr.

The analysis is conducted using the full feature THM model, but to eliminate the effect of solid phase deformation, the elastic modulus is made relatively high (= 10 GPa). The material parameters and constitutive relationships as given by Grenier et al. (2018) are implemented, except for the water and ice properties, for which we utilized the water equation of state given in Appendix A. The water and ice properties in the reference benchmark are treated as constants.

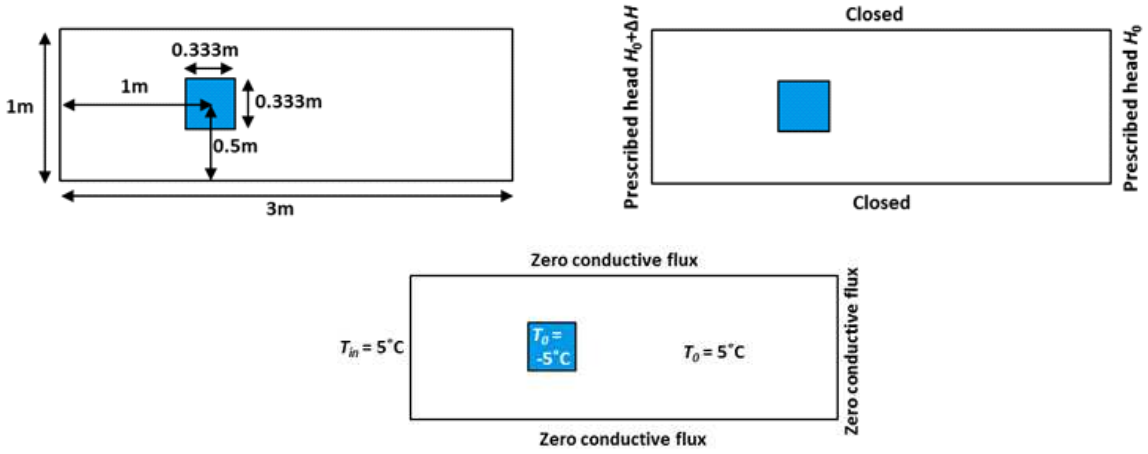

Fig. 1 Geometry and initial and boundary conditions of the TH2 benchmark case.

The finite element domain is discretized using 2D linear, quadrilateral finite elements. The analysis is conducted on half of the domain, using two mesh sizes: 374 and 1134 elements. Fig. 2 shows the computational results at 22,860 s and later, obtained from both meshes. It would have been ideal if the digital file of the reference benchmark had been accessible, but comparing Fig. 2 at 22,860 s to Fig. 2b (P. 200 of Grenier et al. (2018)), it can readily be noticed that the two results are very close. The small difference, however, can be attributed to the way the ice and water properties are defined. Also, it can be noticed that the coarse mesh (374 elements) gave rather close results to the finer mesh (1134 elements), indicating that the model is effectively mesh-independent. Both meshes, however, are much smaller than those utilized in solving the reference benchmark.

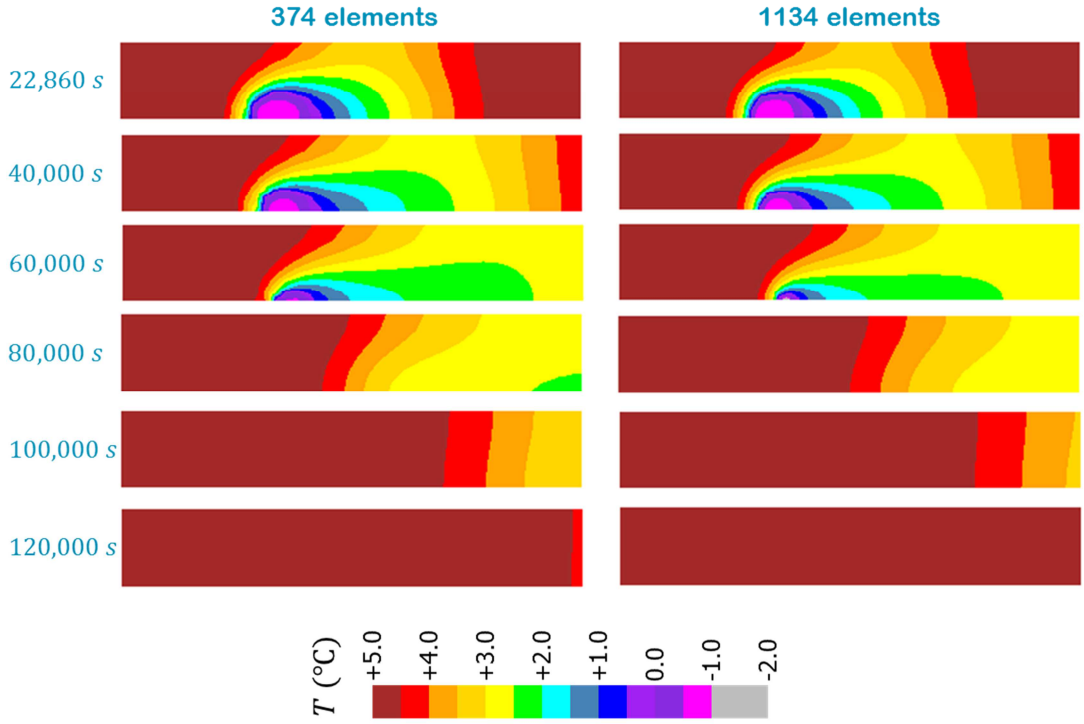

Fig. 2 Temperature evolution at different times using 374 and 1134 elements.

Fig. 3 shows the evolution of the minimum temperature with time. Comparing this figure to Fig. 9a (P. 207 of Grenier et al. (2018)) reveals that the two results are very close and, as mentioned above, the small difference in the results can be attributed to the difference in ice and water properties. The same can be observed in comparing the evolution of the water volume with time, given in Fig. 4, with that in Fig. 9b (P. 207 of Grenier et al. (2018)).

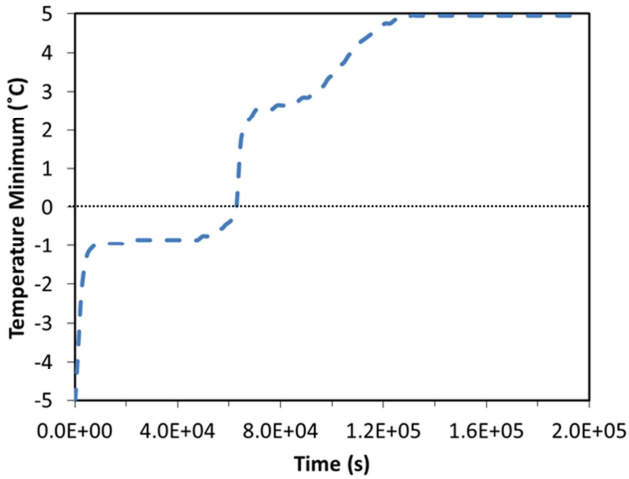

Fig. 3 Evolution of the minimum temperature with time using 1134 elements.

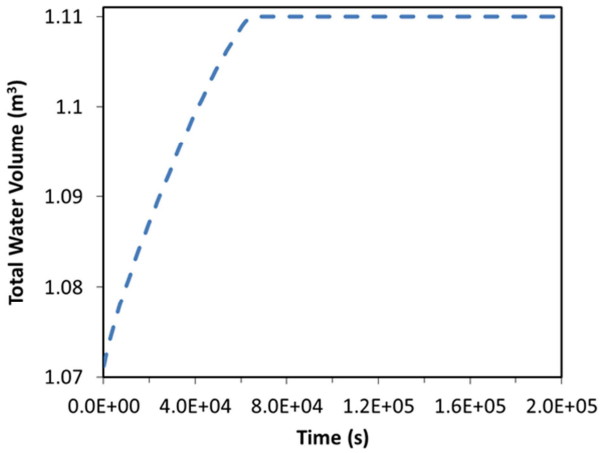

Fig. 4 Evolution of the total water with time using 1134 elements.

Thus, it can be concluded that the introduced THM model is capable of handling cases which are considered to be computationally challenging. However, this verification exercise does not reflect all features of the model, and in order to highlight the complete features, a more involved numerical example is given in the next section.

6 Numerical example

A numerical example demonstrating the capabilities of the model to simulate a freezing and thawing cycle in soil is presented. The geometry is designated to resemble a soil mass surrounding an energy

pile. An axial symmetric soil mass, 24.5 m diameter and 12 m deep, subjected to a 10 m long and 0.5 m diameter cylindrical heat source, is simulated. The heat source represents an energy pile coinciding along the symmetrical axis of the soil, as shown in Fig. 5.

Initial and boundary conditions:

Initially, the temperature in the soil mass is assumed 5℃, the pressure is hydrostatic, and the horizontal effective stress is equal to overlying soil mass.

Thermal, mechanical and hydraulic boundary conditions are imposed. The right-hand side boundary is prescribed by: 1) a constant temperature of 5 °C, 2) an overburden pressure equal to the weight of the soil mass, and 3) made hydraulically open for groundwater flow. The top and bottom boundaries are considered thermally insulated and hydraulically closed. The left and bottom boundaries are supported by rollers to restrict the normal displacements to these boundaries. At the contact surface between the soil mass and the heat source, a Cauchy boundary condition, describing a heat flux arising due to their thermal interaction, is imposed as

$$Q = b\left(T_s - T_p\right) \tag{71}$$

in which b is the thermal interaction coefficient, and T_p is a prescribed heat source temperature, simulating a 28 days freezing-thawing cycle, shown in Fig. 6.

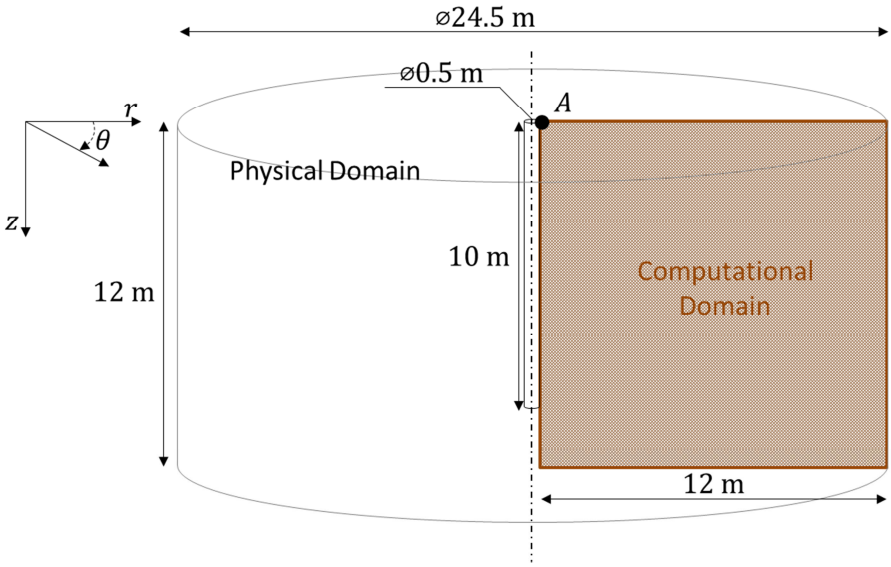

Fig. 5 Physical and computational domains.

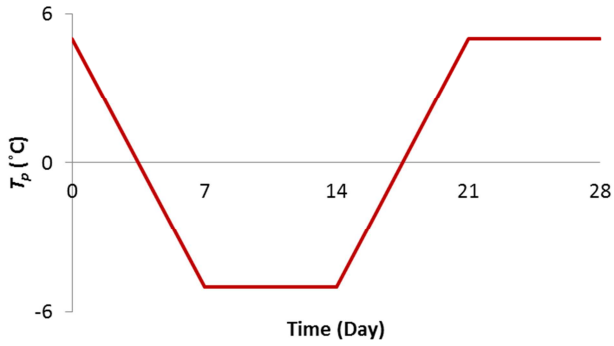

Fig. 6 Pile temperature.

Material parameters and constitutive relationships:

Table 1 lists the physical and thermomechanical properties of the materials.

Fig. 7 shows the soil elastic modulus versus temperature, as given by Eq. (35), and the soil freezing curve (SFC), as given by Eq. (36).

Table 1 Model parameters

Parameter		Value
Solid matrix		
	Reference elastic modulus, $\boldsymbol{E_0}$ (MPa), Eq. (35)	5.0
	Elastic modulus constant, $\boldsymbol{b}$ ($\mathbf{K^{-1}}$), Eq. (35)	0.1
	Poisson's ratio, $\boldsymbol{\nu_s}$ (-)	0.25
	Bulk modulus of soil grains, $\boldsymbol{K_s}$ (MPa)	500.0
	Density, $\boldsymbol{\rho_s}$ ($\mathbf{kg\ m^{-3}}$)	1600.0
	Permeability, $\boldsymbol{k}$ ($\mathbf{m^2}$)	$\mathbf{1.0 \times 10^{-15}}$
	Initial porosity, $\boldsymbol{\varphi}$ (-)	0.3
	Relative permeability parameter, $\boldsymbol{\eta}$ (-), Eq. (40)	7.5
	Heat capacity, $\boldsymbol{c_{ps}}$ ($\mathbf{J\ kg^{-1}\ K^{-1}}$)	900.0
	Thermal conductivity, $\boldsymbol{\lambda_s}$ ($\mathbf{W\ m^{-2}\ K^{-1}}$)	1.0
	SFC constant, $\boldsymbol{a}$ ($\mathbf{K^{-1}}$), Eq. (36)	0.03
	SFC residual unfrozen water, $\boldsymbol{S^*}$ (-), Eq. (36)	0.0
	Thermal expansion coefficient, $\boldsymbol{\beta_s}$, ($\mathbf{K^{-1}}$)	$\mathbf{5.0 \times 10^{-6}}$
	Characteristic length, $\boldsymbol{\ell_c}$ (m), Eq. (66)	0.05
Water		
	Liquid water and ice properties	Appendix A
Pile		
	Thermal interaction coefficient $\boldsymbol{b}$ ($\boldsymbol{W\ m^{-2}\ K^{-1}}$)	20.0

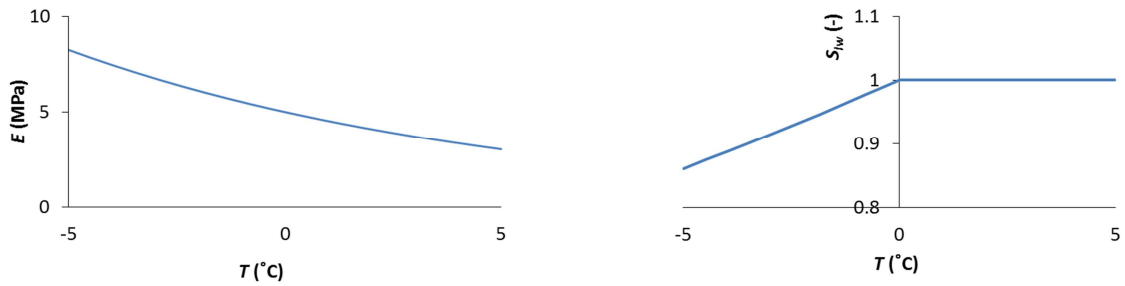

(a) (b)

Fig. 7 (a) Soil elastic modulus, (b) Soil freezing curve (SFC).

Finite element analysis:

The finite element domain is discretized using 400 linear quadrilateral axisymmetric finite elements. The axial symmetric finite element is formulated by solving the finite element system of equations, Eq. (69), in the cylindrical coordinate system (r, z).

Fig. 8 shows the computational results for temperature, cryogenic suction, porosity expansion and deformed mesh at three instants in time: just before freezing ($t = 5\ days$); during freezing ($t = 14\ days$); and just after freezing ($t = 19\ days$). Fig. 8a shows that as the temperature is above freezing point, there is no sign of cryogenic suction and the porosity expansion and solid matrix heaving are minimal. Fig. 8b shows that upon freezing, the cryogenic suction arises, associated with porosity expansion and frost heaving. Fig. 8c shows that by thawing, the cryogenic suction disappears, and the porosity and heaving are decreased.

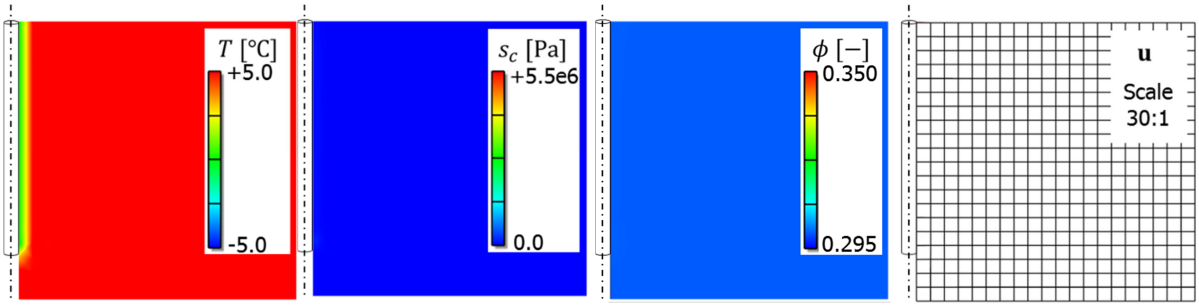

(a)

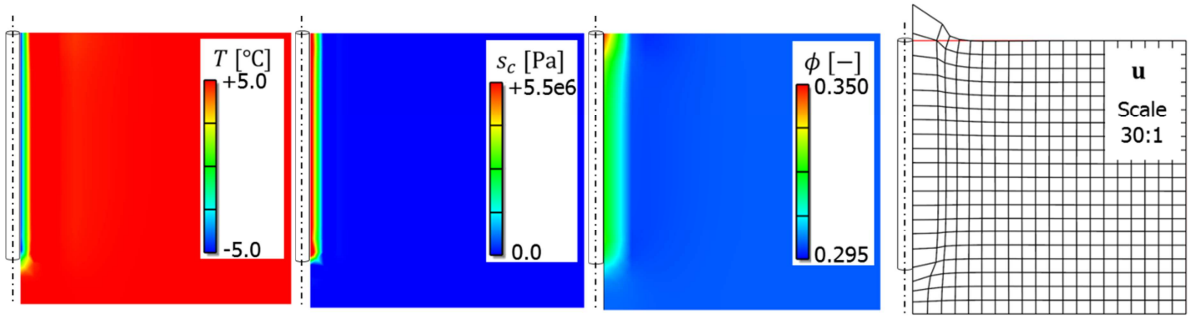

(b)

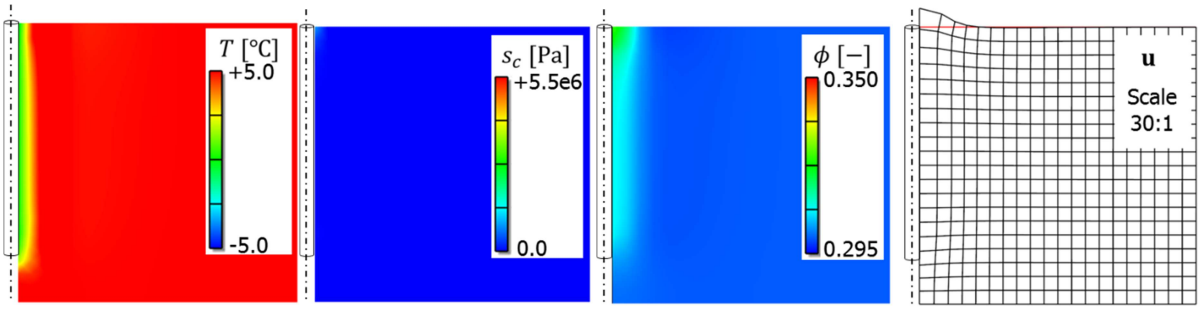

(c)

Fig. 8 Computational results for temperatures, cryogenic suctions, porosities, and deformed mesh: (a) just before freezing ($t = 5\ days$), (b) during freezing ($t = 14\ days$), (c) just after freezing ($t = 19\ days$).

Fig. 9 shows the temporal evolution of temperature, cryogenic suction, porosity and heaving at point $A(r = 0.25\ \text{m}, z = 0.0\ \text{m})$, shown in Fig. 5, at the surface. Fig. 9a shows the evolution of temperature, which reaches its minimum value of $-4.9℃$ after 14 days, followed by an increase in response to the temperature increase in the heat source. Fig. 9b shows the evolution of cryogenic suction with its value reaches its maximum of 5.5 MPa (55 bar) after 14 days, in association with the minimum temperature. Fig. 9c shows the evolution of porosity, which closely follows the evolution of cryogenic suction. The maximum reached porosity is $\varphi = 0.35$, an increase of 17% of its initial value of 0.3. With thawing, the porosity reduces to 0.33 after 19 days, keeping some of the migrated moisture, but, after 28 days, it becomes 0.3005, almost contracted to its initial value. Fig. 9d shows the frost heaving at point A. It shows that it evolves in association with the onset of cryosuction and pore expansion. Upon freezing, it reached $-u_z = 0.052$ m, but during thawing most of the heave has been reversed and the remaining heave after 19 days is 0.033 m and after 28 days is 0.002 m. Apparently, the nearly full reverse of the heave is due to the use of an elastic constitutive model for the solid phase. Caicedo (2017) has shown experimentally that during thawing, the fine sand exhibits nearly full reversal of heave, but the silt is irreversible, leaving a considerable residual heave. This difference in behavior among different soil materials necessitates the use of a proper elasto-plastic model to simulate accurately the behavior under different freezing and thawing boundary conditions.

Fig. 10 shows the water flow vectors after 5 days (just before freezing) and after 14 days (at the peak of freezing). The figure shows that before freezing, the water migrates from the cold region to the warm region due to its volumetric expansion, but by the onset of freezing, the water flows back to the frozen region due to cryogenic suction.

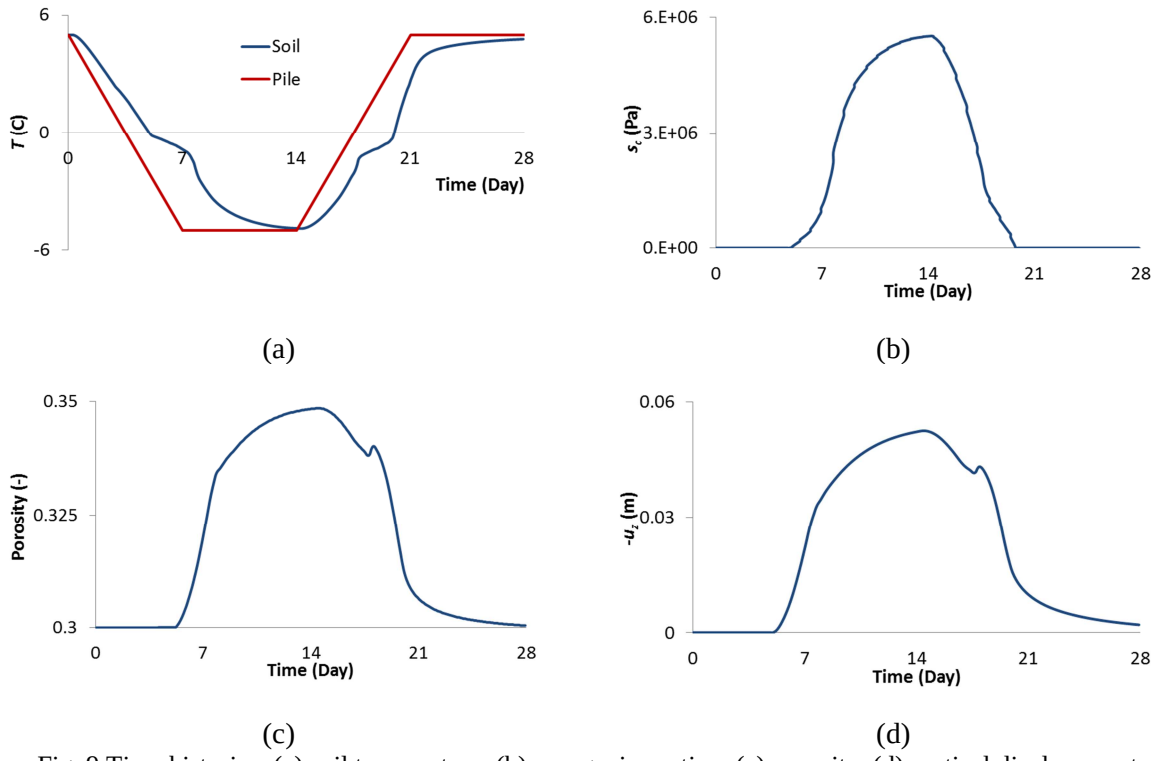

Fig. 9 Time histories: (a) soil temperature, (b) cryogenic suction, (c) porosity, (d) vertical displacement.

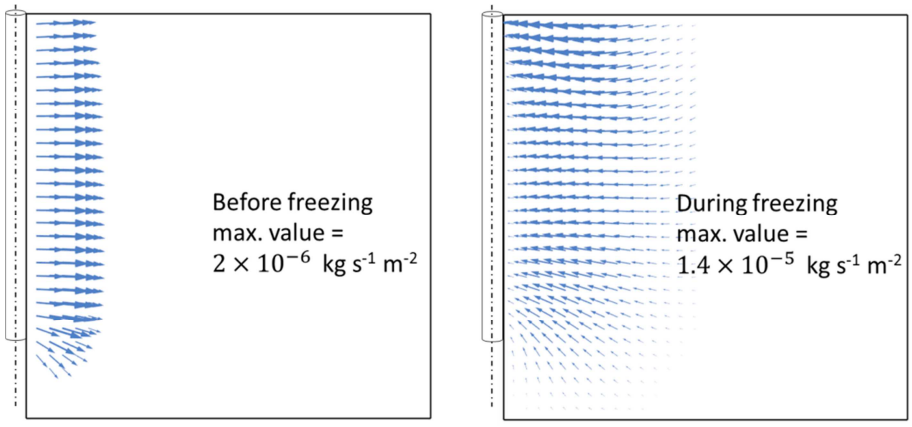

(a) (b)

Fig. 10 Water mass flow vectors: (a) t = 5 days, (b) t = 14 days.

Fig. 11 shows the spatial distribution of temperature, cryogenic suction, porosity, frost heaving, ice saturation, and liquid water pressure, computed at the boundary along the heat source on six instants in times: $t = 0, 5, 7, 8, 14, 19\ days$, where $t = 0$ represents the initial condition, $t = 5\ days$ represents the time just before freezing, $t = 7 - 14\ days$ represents the time during freezing and $t = 19\ days$ represents the time just after thawing. The figure demonstrates the strong coupling between the involved phenomena, which follow firmly the evolution of temperature. An interesting observation can be noticed in Fig. 11a where, during freezing on days 7 and 8, there is a time lag in the advancement of freezing at the upper side of the domain as compared to the lower side. This can be attributed to the substantial expansion of porosity in this area, as shown in Fig. 11c. The porosity expansion is associated with the migration of unfrozen water from the warm region to the frozen region due to cryosuction, giving rise to a warmer temperature. Another interesting observation can be seen in Fig. 11d, where it shows that there is a neutral heaving point at around $z = 7m$. Above this point, the soil exhibits heaving due to the coupling effect between porosity expansion, water volume expansion and the increase of water contents due to cryosuction. Below this point, the soil exhibits contraction due to the overburden pressure. Fig. 11f shows that before freezing, the liquid water pressure is hydrostatic, but after freezing, it becomes negative due to the cryogenic suction.

Examining the computational results reveals that the model is capable of capturing the strong coupling between thermo-hydro-mechanical phenomena occurring during freezing and thawing in soil. A noteworthy feature of the model is the capturing of the jump in the cryogenic suction and its associated porosity expansion and frost heaving. Capturing such a behavior using a relatively coarse mesh was feasible by two main attributes. The first attribute is the choice of the primary state variables, especially the inclusion of the cryosuction s_c among them. And the second attribute is the use of the mixed discretization scheme, where s_c is discretized using the partition of unity method. If use is made of the standard finite element method, the jump in the cryogenic suction would not be possible to capture and its value would be underestimated. This is shown in Fig. 12 where all primary state variables are discretized using the standard Galerkin finite element method. The figure shows that after 14 days of freezing, there is no jump in the cryogenic suction, as compared to Fig. 8b, and its

maximum magnitude is 3.6 MPa. Theoretically, as per Eq. (37), the cryogenic suction at $-4.9℃$ should be 5.5 $MPa \equiv 55\ bar$.

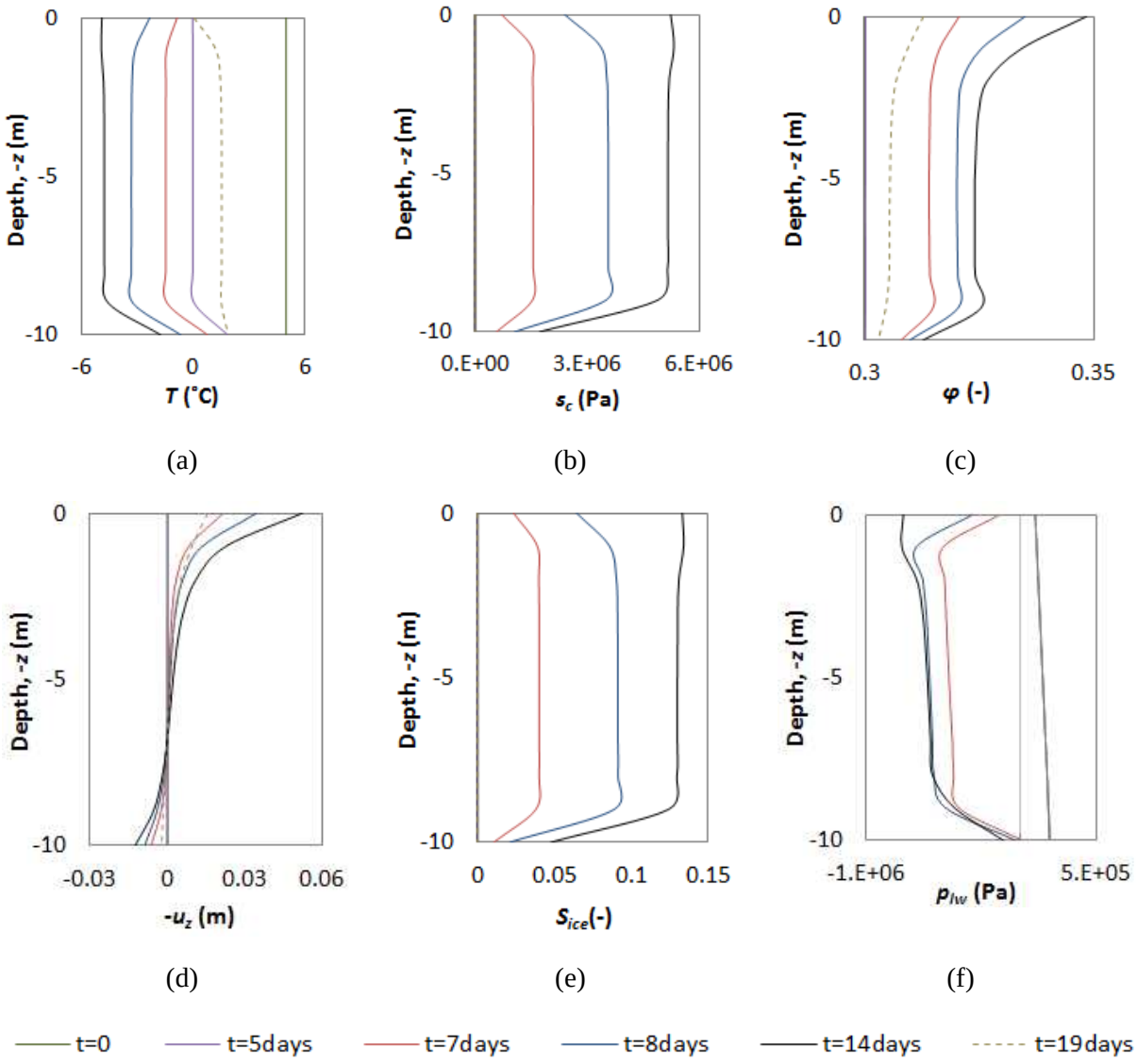

Fig. 11 Field variables along the boundary with the energy pile: (a) soil temperature, (b) cryogenic suction, (c) porosity, (d) vertical displacement, (e) ice saturation, (f) liquid water pressure.

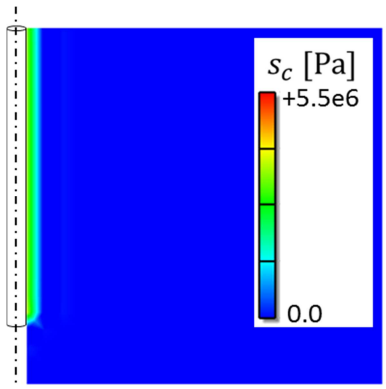

Fig. 12 Standard FEM with 400 elements. Cryosuction at Day 14.

7 Conclusions

This paper presents a computational model capable of simulating the strong coupling between all important thermo-hydro-mechanical phenomena occurring during freezing and thawing of a porous domain resembling a soil mass surrounding an energy pile. The model is formulated based on the averaging theory and discretized using the finite element method.

Three features make the proposed model distinct from others: the mathematical formulation of the physics, the choice of the primary state variables and the discretization scheme. A comprehensive mathematical formulation is employed to describe all important phenomena and processes in freezing-thawing of porous media, including solid and fluid compressibility, buoyancy, phase change, thermomechanical behavior, water volume change, pores expansion, cryogenic suction, melting point depression and water migration to the freezing zone. The use of fundamental balance equations within the framework of the averaging theory, together with the equations of state of water and generic ice-water constitutive relationships make the modeled physics rather wide-ranging.

In current THM models, the primary state variables are typically solid displacement, pore pressure and temperature. The use of these variables might be adequate for slow freezing rates, which is the case in nature, but for a relatively high freezing rate, such as in artificial ground freezing or shallow geothermal systems, this choice of state variables would most probably cause critical spurious oscillations, unless treated properly. Na and Sun (2017) thoroughly discussed this issue, and asserted that the performance of their model was improved only after employing a stabilization technique in the weighted-residuals of the mass and energy balance equations. In this work, we demonstrated that treating the cryogenic suction as a primary state variable alleviates this problem, and in this case even the standard Galerkin finite element method (SG) can handle relatively high freezing-thawing rate problems. However, as discussed in Section 5 and shown in Fig. 12, SG falls short from capturing the rapid rise of the cryogenic suction, but tends to smear it. We tackled this issue by discretizing the cryogenic suction using the partition of unity method. The governing equations are solved using a mixed finite element discretization scheme, where the continuous and smooth primary state variables, namely, the solid phase displacement, water mixture pressure, water mixture specific enthalpy, and solid specific enthalpy are discretized using the standard Galerkin finite element method, and the cryogenic suction is discretized using the partition of unity within the framework of XFEM. This combination has enabled the simulation of a relatively high freezing-thawing rate problem, and resulted into an accurate, robust and effectively mesh-independent numerical scheme.

Acknowledgements

The authors acknowledge the financial support by NWO (Netherlands Organization for Scientific Research) under grant number 14698. They highly appreciate FUNDEX (piles company), Deltares (geotechnics consultancy company) and TNO DIANA (finite element company) for their in-kind contributions and technical support; and the Green Village of Delft for accommodating the energy pile.

Appendix A: Water equations of state

The water equations of state (EOS) for subcooled liquid water, supercooled water and ice are formulated from relevant references, given below.

Subcooled liquid water:

Specific heat capacity (IAPWS 2007):

$$c_p = -R_{\mathrm{H2O}} T_m^{*2} \frac{\partial^2 \gamma}{\partial p_m^{*2}}$$

in which R_{H2O} is specific gas constant for water, $p_m^* = p_m / 16.53\times10^6$, $T_m^* = 1386.0 / T_m$ and

$$\gamma\left(p_m^*, T_m^*\right) = \sum_{i=1}^{34} n_i \left(7.1 - p_m^*\right)^{I_i} \left(T_m^* - 1.222\right)^{J_i}$$

where n_i, I_i and J_i are material constants.

Density (IAPWS 2007):

$$\rho = \frac{p_m}{R_{\mathrm{H2O}} T_m p_m^* \dfrac{\partial \gamma}{\partial p_m^*}}$$

Viscosity (Cooper and Dooley 2008):

$$\mu = \frac{100\sqrt{T_m / 647.096}}{\displaystyle\sum_{i=0}^{3} \frac{H_i}{\left(T_m / 647.096\right)^i}} e^{\frac{\rho}{322.0}\sum_{i=0}^{5}\left(\frac{647.096}{T_m}-1\right)^i \sum_{j=0}^{6} H_{ij}\left(\frac{\rho}{322.0}-1\right)^j} e^{0.068Y}$$

where Y, H_i and H_{ij} are material constants.

Heat conductivity (Ramires et al. 1994):

$$\lambda = 0.6065\left(-1.48445 + 4.12292\left(\frac{T_m}{298.15}\right) - 1.63866\left(\frac{T_m}{298.15}\right)^2\right)$$

Supercooled liquid water:

Specific heat capacity (Tombari et al. 1999):

$$c_p = \frac{1}{18.01528\times10^{-3}}\left[0.044\left(\frac{T_m}{222} - 1\right)^{-2.5} + 74.3\right]$$

Density (Hare and Sorensen 1987):

$$\rho = -0.0228\left(T_m - 273.15\right)^2 - 0.1176\left(T_m - 273.15\right) + 999.9$$

Viscosity (Hallett 1963):

$$\mu = 5.0\times10^{-6}\left(T_m - 273.15\right)^2 - 3.0\times10^{-5}\left(T_m - 273.15\right) + 0.0018$$

Heat conductivity (Benchikh et al. 1985):

$$\lambda = 0.0017\left(T_m - 273.15\right) + 0.5583$$

Ice:

Specific heat capacity (Fukusako 1990):

$$c_p = 185.0 + 6.89\left(T_m - 273.15\right)$$

Density (Fukusako 1990):

$$\rho = 917.0\left(1. - 1.17\times10^{-4}\left(T_m - 273.15\right)\right)$$

Heat conductivity (Fukusako 1990):

$$\lambda = 1.16\left(1.91 - 8.66\times10^{-3}\left(T_m - 273.15\right) + 2.97\times10^{-5}\left(T_m - 273.15\right)^2\right)$$

Appendix B: Linearized balance equations

The linearized balance equations from Section 4.2 are:

Momentum balance:

$$
\begin{aligned}
&-\int_\Omega \mathbf{L}^T w\mathbf{D}_s\mathbf{L}\dot{\mathbf{u}}^r d\Omega - \int_\Omega \mathbf{L}^T w\mathbf{D}_s\mathbf{L}\delta\dot{\mathbf{u}}\ d\Omega + \int_\Omega \mathbf{L}^T w\mathbf{D}_s \frac{1}{3}\mathbf{m}\beta_s \frac{1}{c_{ps}}\dot{h}_s^r d\Omega + \int_\Omega \mathbf{L}^T w\mathbf{D}_s \frac{1}{3}\mathbf{m}\beta_s \frac{1}{c_{ps}}\delta\dot{h}_s d\Omega \\
&+ \int_\Omega \mathbf{L}^T w\mathbf{m}\alpha\left(\frac{\partial p_s}{\partial h_m}\right)^r \dot{h}_m^r d\Omega + \int_\Omega \mathbf{L}^T w\mathbf{m}\alpha\left(\frac{\partial p_s}{\partial h_m}\right)^r \delta\dot{h}_m d\Omega + \int_\Omega \mathbf{L}^T w\mathbf{m}\alpha\left(\frac{\partial^2 p_s}{\partial {h_m}^2}\right)^r \dot{h}_m^r \delta h_m d\Omega \\
&+ \int_\Omega \mathbf{L}^T w\mathbf{m}\alpha\left(\frac{\partial^2 p_s}{\partial h_m \partial p_m}\right)^r \dot{h}_m^r \delta p_m d\Omega + \int_\Omega \mathbf{L}^T w\mathbf{m}\alpha\left(\frac{\partial^2 p_s}{\partial h_m \partial s_c}\right)^r \dot{h}_m^r \delta s_c d\Omega \\
&+ \int_\Omega \mathbf{L}^T w\mathbf{m}\alpha\left(\frac{\partial p_s}{\partial p_m}\right)^r \dot{p}_m^r d\Omega + \int_\Omega \mathbf{L}^T w\mathbf{m}\alpha\left(\frac{\partial p_s}{\partial p_m}\right)^r \delta\dot{p}_m d\Omega + \int_\Omega \mathbf{L}^T w\mathbf{m}\alpha\left(\frac{\partial^2 p_s}{\partial p_m \partial h_m}\right)^r \dot{p}_m^r \delta h_m d\Omega \\
&+ \int_\Omega \mathbf{L}^T w\mathbf{m}\alpha\left(\frac{\partial^2 p_s}{\partial {p_m}^2}\right)^r \dot{p}_m^r \delta p_m d\Omega + \int_\Omega \mathbf{L}^T w\mathbf{m}\alpha\left(\frac{\partial^2 p_s}{\partial p_m \partial s_c}\right)^r \dot{p}_m^r \delta s_c d\Omega \\
&+ \int_\Omega \mathbf{L}^T w\mathbf{m}\alpha\left(\frac{\partial p_s}{\partial s_c}\right)^r \dot{s}_c^r d\Omega + \int_\Omega \mathbf{L}^T w\mathbf{m}\alpha\left(\frac{\partial p_s}{\partial s_c}\right)^r \delta\dot{s}_c d\Omega + \int_\Omega \mathbf{L}^T w\mathbf{m}\alpha\left(\frac{\partial^2 p_s}{\partial s_c \partial h_m}\right)^r \dot{s}_c^r \delta h_m d\Omega \\
&+ \int_\Omega \mathbf{L}^T w\mathbf{m}\alpha\left(\frac{\partial^2 p_s}{\partial s_c \partial p_m}\right)^r \dot{s}_c^r \delta p_m d\Omega + \int_\Omega \mathbf{L}^T w\mathbf{m}\alpha\left(\frac{\partial^2 p_s}{\partial {s_c}^2}\right)^r \dot{s}_c^r \delta s_c d\Omega + \int_\Omega w\left(\frac{\partial \rho_{eff}}{\partial h_m}\right)^r \dot{h}_m^r \mathbf{g} d\Omega \\
&+ \int_\Omega w\left(\frac{\partial \rho_{eff}}{\partial h_m}\right)^r \delta\dot{h}_m \mathbf{g} d\Omega + \int_\Omega w\left(\frac{\partial^2 \rho_{eff}}{\partial {h_m}^2}\right)^r \dot{h}_m^r \delta h_m \mathbf{g} d\Omega + \int_\Omega w\left(\frac{\partial^2 \rho_{eff}}{\partial h_m \partial p_m}\right)^r \dot{h}_m^r \delta p_m \mathbf{g} d\Omega \\
&+ \int_\Omega w\left(\frac{\partial \rho_{eff}}{\partial p_m}\right)^r \dot{p}_m^r \mathbf{g} d\Omega + \int_\Omega w\left(\frac{\partial \rho_{eff}}{\partial p_m}\right)^r \delta\dot{p}_m \mathbf{g} d\Omega + \int_\Omega w\left(\frac{\partial^2 \rho_{eff}}{\partial p_m \partial h_m}\right)^r \dot{p}_m^r \delta h_m \mathbf{g} d\Omega \\
&+ \int_\Omega w\left(\frac{\partial^2 \rho_{eff}}{\partial {p_m}^2}\right)^r \dot{p}_m^r \delta p_m \mathbf{g} d\Omega + \int_{\Gamma_q} w\hat{\dot{\mathbf{t}}} d\Gamma = 0
\end{aligned}
$$

Mass balance:

$$\int_\Omega w d_1^r \dot{p}_m^r d\Omega + \int_\Omega w d_1^r \delta \dot{p}_m d\Omega + \int_\Omega w \left(\frac{\partial d_1}{\partial h_m}\right)^r \dot{p}_m^r \delta h_m d\Omega + \int_\Omega w \left(\frac{\partial d_1}{\partial p_m}\right)^r \dot{p}_m^r \delta p_m d\Omega$$
$$+ \int_\Omega w \left(\frac{\partial d_1}{\partial s_c}\right)^r \dot{p}_m^r \delta s_c d\Omega + \int_\Omega w d_2^r \dot{h}_m^r d\Omega + \int_\Omega w d_2^r \delta \dot{h}_m d\Omega + \int_\Omega w \left(\frac{\partial d_2}{\partial h_m}\right)^r \dot{h}_m^r \delta h_m d\Omega$$
$$+ \int_\Omega w \left(\frac{\partial d_2}{\partial p_m}\right)^r \dot{h}_m^r \delta p_m d\Omega + \int_\Omega w \left(\frac{\partial d_2}{\partial s_c}\right)^r \dot{h}_m^r \delta s_c d\Omega + \int_\Omega w d_3^r \dot{h}_s^r d\Omega + \int_\Omega w d_3^r \delta \dot{h}_s d\Omega$$
$$+ \int_\Omega w \left(\frac{\partial d_3}{\partial h_m}\right)^r \dot{h}_s^r \delta h_m d\Omega + \int_\Omega w \left(\frac{\partial d_3}{\partial p_m}\right)^r \dot{h}_s^r \delta p_m d\Omega + \int_\Omega w d_4^r \mathbf{m}^T \mathbf{L} \dot{\mathbf{u}}^r d\Omega$$
$$+ \int_\Omega w d_4^r \mathbf{m}^T \mathbf{L} \delta \dot{\mathbf{u}} \; d\Omega + \int_\Omega w \left(\frac{\partial d_4}{\partial h_m}\right)^r \mathbf{m}^T \mathbf{L} \dot{\mathbf{u}}^r \delta h_m d\Omega + \int_\Omega w \left(\frac{\partial d_4}{\partial p_m}\right)^r \mathbf{m}^T \mathbf{L} \dot{\mathbf{u}}^r \delta p_m d\Omega$$
$$+ \int_\Omega w e_1^r \dot{s}_c^r d\Omega + \int_\Omega w e_1^r \delta \dot{s}_c d\Omega + \int_\Omega w \left(\frac{\partial e_1}{\partial h_m}\right)^r \dot{s}_c^r \delta h_m d\Omega + \int_\Omega w \left(\frac{\partial e_1}{\partial p_m}\right)^r \dot{s}_c^r \delta p_m d\Omega$$
$$+ \int_\Omega w \left(\frac{\partial e_1}{\partial s_c}\right)^r \dot{s}_c^r \delta s_c d\Omega + \int_\Omega \nabla w \cdot \mathbf{c}_1^r \nabla p_m^r d\Omega + \int_\Omega \nabla w \cdot \mathbf{c}_1^r \delta \nabla p_m d\Omega$$
$$+ \int_\Omega \nabla w \cdot \left(\frac{\partial \mathbf{c}_1}{\partial h_m}\right)^r \nabla p_m^r \delta h_m d\Omega + \int_\Omega \nabla w \cdot \left(\frac{\partial \mathbf{c}_1}{\partial p_m}\right)^r \nabla p_m^r \delta p_m d\Omega + \int_\Omega \nabla w \cdot \mathbf{c}_2^r \nabla s_c^r d\Omega$$
$$+ \int_\Omega \nabla w \cdot \mathbf{c}_2^r \delta \nabla s_c d\Omega + \int_\Omega \nabla w \cdot \left(\frac{\partial \mathbf{c}_2}{\partial h_m}\right)^r \nabla s_c^r \delta h_m d\Omega + \int_\Omega \nabla w \cdot \left(\frac{\partial \mathbf{c}_2}{\partial p_m}\right)^r \nabla s_c^r \delta p_m d\Omega$$
$$- \int_\Omega \nabla w \cdot \mathbf{G}_1^r d\Omega - \int_\Omega \nabla w \cdot \left(\frac{\partial \mathbf{G}_1}{\partial h_m}\right)^r \delta h_m d\Omega - \int_\Omega \nabla w \cdot \left(\frac{\partial \mathbf{G}_1}{\partial p_m}\right)^r \delta p_m d\Omega + \int_{\Gamma_q} w \hat{q}_{lw} d\Gamma = 0$$

Energy balance:

$$\int_\Omega w d_5^r \dot{h}_s^r d\Omega + \int_\Omega w d_5^r \delta \dot{h}_s d\Omega + \int_\Omega w \left(\frac{\partial d_5}{\partial h_m}\right)^r \dot{h}_s^r \delta h_m d\Omega + \int_\Omega w \left(\frac{\partial d_5}{\partial p_m}\right)^r \dot{h}_s^r \delta p_m d\Omega$$
$$+ \int_\Omega w d_6^r \dot{h}_m^r d\Omega + \int_\Omega w d_6^r \delta \dot{h}_m d\Omega + \int_\Omega w \left(\frac{\partial d_6}{\partial h_m}\right)^r \dot{h}_m^r \delta h_m d\Omega + \int_\Omega w \left(\frac{\partial d_6}{\partial p_m}\right)^r \dot{h}_m^r \delta p_m d\Omega$$
$$+ \int_\Omega w \left(\frac{\partial d_6}{\partial s_c}\right)^r \dot{h}_m^r \delta s_c d\Omega + \int_\Omega w d_7^r \dot{p}_m^r d\Omega + \int_\Omega w d_7^r \delta \dot{p}_m d\Omega + \int_\Omega w \left(\frac{\partial d_7}{\partial h_m}\right)^r \dot{p}_m^r \delta h_m d\Omega$$
$$+ \int_\Omega w \left(\frac{\partial d_7}{\partial p_m}\right)^r \dot{p}_m^r \delta p_m d\Omega + \int_\Omega w \left(\frac{\partial d_7}{\partial s_c}\right)^r \dot{p}_m^r \delta s_c d\Omega + \int_\Omega w d_8^r \mathbf{m}^T \mathbf{L} \dot{\mathbf{u}}^r d\Omega$$
$$+ \int_\Omega w d_8^r \mathbf{m}^T \mathbf{L} \delta \dot{\mathbf{u}} \; d\Omega + \int_\Omega w \left(\frac{\partial d_8}{\partial h_m}\right)^r \mathbf{m}^T \mathbf{L} \dot{\mathbf{u}}^r \delta h_m d\Omega + \int_\Omega w \left(\frac{\partial d_8}{\partial p_m}\right)^r \mathbf{m}^T \mathbf{L} \dot{\mathbf{u}}^r \delta p_m d\Omega$$
$$+ \int_\Omega w \left(\frac{\partial d_8}{\partial h_s}\right)^r \mathbf{m}^T \mathbf{L} \dot{\mathbf{u}}^r \delta h_s d\Omega + \int_\Omega w e_2^r \dot{s}_c^r d\Omega + \int_\Omega w e_2^r \delta \dot{s}_c d\Omega + \int_\Omega w \left(\frac{\partial e_2}{\partial h_m}\right)^r \dot{s}_c^r \delta h_m d\Omega$$
$$+ \int_\Omega w \left(\frac{\partial e_2}{\partial p_m}\right)^r \dot{s}_c^r \delta p_m d\Omega + \int_\Omega w \left(\frac{\partial e_2}{\partial s_c}\right)^r \dot{s}_c^r \delta s_c d\Omega + \int_\Omega \nabla w \cdot \mathbf{c}_3^r \nabla p_m^r d\Omega$$
$$+ \int_\Omega \nabla w \cdot \mathbf{c}_3^r \delta \nabla p_m d\Omega + \int_\Omega \nabla w \cdot \left(\frac{\partial \mathbf{c}_3}{\partial h_m}\right)^r \nabla p_m^r \delta h_m d\Omega + \int_\Omega \nabla w \cdot \left(\frac{\partial \mathbf{c}_3}{\partial p_m}\right)^r \nabla p_m^r \delta p_m d\Omega$$
$$+ \int_\Omega \nabla w \cdot \mathbf{c}_4^r \nabla s_c^r d\Omega + \int_\Omega \nabla w \cdot \mathbf{c}_4^r \delta \nabla s_c d\Omega + \int_\Omega \nabla w \cdot \left(\frac{\partial \mathbf{c}_4}{\partial h_m}\right)^r \nabla s_c^r \delta h_m d\Omega$$
$$+ \int_\Omega \nabla w \cdot \left(\frac{\partial \mathbf{c}_4}{\partial p_m}\right)^r \nabla s_c^r \delta p_m d\Omega + \int_\Omega \nabla w \cdot \mathbf{c}_5^r \nabla h_s^r d\Omega + \int_\Omega \nabla w \cdot \mathbf{c}_5^r \delta \nabla h_s d\Omega$$
$$+ \int_\Omega \nabla w \cdot \left(\frac{\partial \mathbf{c}_5}{\partial h_m}\right)^r \nabla h_s^r \delta h_m d\Omega + \int_\Omega \nabla w \cdot \left(\frac{\partial \mathbf{c}_5}{\partial p_m}\right)^r \nabla h_s^r \delta p_m d\Omega - \int_\Omega \nabla w \cdot \mathbf{G}_2^r d\Omega$$
$$- \int_\Omega \nabla w \cdot \left(\frac{\partial \mathbf{G}_2}{\partial h_m}\right)^r \delta h_m d\Omega - \int_\Omega \nabla w \cdot \left(\frac{\partial \mathbf{G}_2}{\partial p_m}\right)^r \delta p_m d\Omega + \int_{\Gamma_q} w \hat{Q}_{\text{adv}} d\Gamma + \int_{\Gamma_q} w \hat{Q}_{\text{cond}} d\Gamma = 0$$

Local thermal equilibrium constraint:

$$\int_\Omega w \frac{1}{c_{ps}} h_s^r d\Omega + \int_\Omega w \frac{1}{c_{ps}} \delta h_s d\Omega$$
$$- \int_\Omega w T_m^r d\Omega - \int_\Omega w \left(\frac{\partial T_m}{\partial h_m}\right)^r \delta h_m d\Omega - \int_\Omega w \left(\frac{\partial T_m}{\partial p_m}\right)^r \delta p_m d\Omega = 0$$

Cryosuction constraint:

Continuous:

$$\int_\Omega w f_{sc}^r d\Omega + \int_\Omega w\left(\frac{\partial f_{sc}}{\partial h_m}\right)^r \delta h_m d\Omega + \int_\Omega w\left(\frac{\partial f_{sc}}{\partial p_m}\right)^r \delta p_m d\Omega - \int_\Omega w s_c^r d\Omega - \int_\Omega w \delta s_c d\Omega = 0$$

Enhanced:

$$\int_\Omega w^* f_{sc}^r d\Omega + \int_\Omega w^*\left(\frac{\partial f_{sc}}{\partial h_m}\right)^r \delta h_m d\Omega + \int_\Omega w^*\left(\frac{\partial f_{sc}}{\partial p_m}\right)^r \delta p_m d\Omega - \int_\Omega w^* s_c^r d\Omega - \int_\Omega w^* \delta s_c d\Omega = 0$$

Appendix C: Components of FE matrices and vectors (Eq. (69))

$\mathbf{K^0}$ submatrices

$$\mathbf{K}_{1-1}^0 = \mathbf{K}_{1-2}^0 = \mathbf{K}_{1-3}^0 = \mathbf{K}_{1-4}^0 = \mathbf{K}_{1-5}^0 = \mathbf{K}_{1-6}^0 = 0 \quad ; \quad \mathbf{K}_{2-1}^0 = \mathbf{K}_{2-3}^0 = \mathbf{K}_{2-4}^0 = 0$$

$$\mathbf{K}_{2-2}^0 = \int_\Omega \nabla \mathbf{N}^T \cdot \mathbf{c}_1^r \nabla \mathbf{N} d\Omega \quad ; \quad \mathbf{K}_{2-5}^0 = \int_\Omega \nabla \mathbf{N}^T \cdot \mathbf{c}_2^r \nabla \mathbf{N} d\Omega \quad ; \quad \mathbf{K}_{2-6}^0 = \int_\Omega \nabla \mathbf{N}^T \cdot \mathbf{c}_2^r \nabla \mathbf{N}^* d\Omega$$

$$\mathbf{K}_{3-1}^0 = \mathbf{K}_{3-3}^0 = 0 \quad ; \quad \mathbf{K}_{3-2}^0 = \int_\Omega \nabla \mathbf{N}^T \cdot \mathbf{c}_3^r \nabla \mathbf{N} d\Omega \quad ; \quad \mathbf{K}_{3-4}^0 = \int_\Omega \nabla \mathbf{N}^T \cdot \mathbf{c}_5^r \nabla \mathbf{N} d\Omega$$

$$\mathbf{K}_{3-5}^0 = \int_\Omega \nabla \mathbf{N}^T \cdot \mathbf{c}_4^r \nabla \mathbf{N} d\Omega \quad ; \quad \mathbf{K}_{3-6}^0 = \int_\Omega \nabla \mathbf{N}^T \cdot \mathbf{c}_4^r \nabla \mathbf{N}^* d\Omega$$

$$\mathbf{K}_{4-1}^0 = \mathbf{K}_{4-2}^0 = \mathbf{K}_{4-3}^0 = \mathbf{K}_{4-5}^0 = \mathbf{K}_{4-6}^0 = 0 \quad ; \quad \mathbf{K}_{4-4}^0 = \int_\Omega \mathbf{N}^T \frac{1}{c_{ps}} \mathbf{N} d\Omega$$

$$\mathbf{K}_{5-1}^0 = \mathbf{K}_{5-2}^0 = \mathbf{K}_{5-3}^0 = \mathbf{K}_{5-4}^0 = \mathbf{K}_{5-5}^0 = \mathbf{K}_{5-6}^0 = 0$$

$$\mathbf{K}_{6-1}^0 = \mathbf{K}_{6-2}^0 = \mathbf{K}_{6-3}^0 = \mathbf{K}_{6-4}^0 = \mathbf{K}_{6-5}^0 = \mathbf{K}_{6-6}^0 = 0$$

$\mathbf{C}^0$ submatrices

$$\mathbf{C}^0_{1-1} = -\int_\Omega \mathbf{B}^T \mathbf{D}_s \mathbf{B} d\Omega \quad ; \quad \mathbf{C}^0_{1-2} = \int_\Omega \mathbf{B}^T \mathbf{m}\alpha \left(\frac{\partial p_s}{\partial p_m}\right)^r \mathbf{N} d\Omega + \int_\Omega \mathbf{N}_u^T \left(\frac{\partial \rho_{eff}}{\partial p_m}\right)^r \mathbf{g}\mathbf{N} d\Omega$$

$$\mathbf{C}^0_{1-3} = \int_\Omega \mathbf{B}^T \mathbf{m}\alpha \left(\frac{\partial p_s}{\partial h_m}\right)^r \mathbf{N} d\Omega + \int_\Omega \mathbf{N}_u^T \left(\frac{\partial \rho_{eff}}{\partial h_m}\right)^r \mathbf{g}\mathbf{N} d\Omega$$

$$\mathbf{C}^0_{1-4} = \int_\Omega \mathbf{B}^T \mathbf{D}_s \frac{1}{3}\mathbf{m}\beta_s \frac{1}{c_{ps}} \mathbf{N} d\Omega \quad ; \quad \mathbf{C}^0_{1-5} = \int_\Omega \mathbf{B}^T \mathbf{m}\alpha \left(\frac{\partial p_s}{\partial s_c}\right)^r \mathbf{N} d\Omega$$

$$\mathbf{C}^0_{1-6} = \int_\Omega \mathbf{B}^T \mathbf{m}\alpha \left(\frac{\partial p_s}{\partial s_c}\right)^r \mathbf{N}^* d\Omega \quad ; \quad \mathbf{C}^0_{2-1} = \int_\Omega \mathbf{N}^T d_4^r \mathbf{m}^T \mathbf{B} d\Omega \quad ; \quad \mathbf{C}^0_{2-2} = \int_\Omega \mathbf{N}^T d_1^r \mathbf{N} d\Omega$$

$$\mathbf{C}^0_{2-3} = \int_\Omega \mathbf{N}^T d_2^r \mathbf{N} d\Omega \quad ; \quad \mathbf{C}^0_{2-4} = \int_\Omega \mathbf{N}^T d_3^r \mathbf{N} d\Omega \quad ; \quad \mathbf{C}^0_{2-5} = \int_\Omega \mathbf{N}^T e_1^r \mathbf{N} d\Omega$$

$$\mathbf{C}^0_{2-6} = \int_\Omega \mathbf{N}^T e_1^r \mathbf{N}^* d\Omega \quad ; \quad \mathbf{C}^0_{3-1} = \int_\Omega \mathbf{N}^T d_8^r \mathbf{m}^T \mathbf{B} d\Omega \quad ; \quad \mathbf{C}^0_{3-2} = \int_\Omega \mathbf{N}^T d_7^r \mathbf{N} d\Omega$$

$$\mathbf{C}^0_{3-3} = \int_\Omega \mathbf{N}^T d_6^r \mathbf{N} d\Omega \quad ; \quad \mathbf{C}^0_{3-4} = \int_\Omega \mathbf{N}^T d_5^r \mathbf{N} d\Omega \quad ; \quad \mathbf{C}^0_{3-5} = \int_\Omega \mathbf{N}^T e_2^r \mathbf{N} d\Omega$$

$$\mathbf{C}^0_{3-6} = \int_\Omega \mathbf{N}^T e_2^r \mathbf{N}^* d\Omega \quad ; \quad \mathbf{C}^0_{4-1} = \mathbf{C}^0_{4-2} = \mathbf{C}^0_{4-3} = \mathbf{C}^0_{4-4} = \mathbf{C}^0_{4-5} = \mathbf{C}^0_{4-6} = 0$$

$$\mathbf{C}^0_{5-1} = \mathbf{C}^0_{5-2} = \mathbf{C}^0_{5-3} = \mathbf{C}^0_{5-4} = \mathbf{C}^0_{5-5} = \mathbf{C}^0_{5-6} = 0$$

$$\mathbf{C}^0_{6-1} = \mathbf{C}^0_{4-2} = \mathbf{C}^0_{6-3} = \mathbf{C}^0_{6-4} = \mathbf{C}^0_{6-5} = \mathbf{C}^0_{6-6} = 0$$

f subvectors

$$\mathbf{f}_1 = -\int_{\Gamma_q} \mathbf{N}_u^T \hat{\mathbf{t}} d\Gamma \quad ; \quad \mathbf{f}_2 = \int_\Omega \nabla \mathbf{N}^T \cdot \mathbf{G}_1^r d\Omega - \int_{\Gamma_q} \mathbf{N}^T \hat{q}_{lw} d\Gamma$$

$$\mathbf{f}_3 = \int_\Omega \nabla \mathbf{N}^T \cdot \mathbf{G}_2^r d\Omega - \int_{\Gamma_q} \mathbf{N}^T \hat{Q}_{\text{adv}} d\Gamma - \int_{\Gamma_q} \mathbf{N}^T \hat{Q}_{\text{cond}} d\Gamma \quad ; \quad \mathbf{f}_4 = \int_\Omega \mathbf{N}^T T_m^r d\Omega$$

$$\mathbf{f}_5 = -\int_\Omega \mathbf{N}^T f_{sc}^r d\Omega \quad ; \quad \mathbf{f}_6 = -\int_\Omega \mathbf{N}^{*T} f_{sc}^r d\Omega$$

K submatrices

$$\mathbf{K}_{1-1} = \mathbf{K}_{1-4} = 0$$

$$\mathbf{K}_{1-2} = \int_\Omega \mathbf{B}^T \mathbf{m} \alpha \left(\frac{\partial^2 p_s}{\partial h_m \partial p_m} \right)^r \dot{h}_m^r \mathbf{N} d\Omega + \int_\Omega \mathbf{B}^T \mathbf{m} \alpha \left(\frac{\partial^2 p_s}{\partial {p_m}^2} \right)^r \dot{p}_m^r \mathbf{N} d\Omega + \int_\Omega \mathbf{B}^T \mathbf{m} \alpha \left(\frac{\partial^2 p_s}{\partial s_c \partial p_m} \right)^r \dot{s}_c^r \mathbf{N} d\Omega$$
$$+ \int_\Omega \mathbf{N}_u^T \left(\frac{\partial^2 \rho_{eff}}{\partial h_m \partial p_m} \right)^r \dot{h}_m^r \mathbf{g} \mathbf{N} d\Omega + \int_\Omega \mathbf{N}_u^T \left(\frac{\partial^2 \rho_{eff}}{\partial {p_m}^2} \right)^r \dot{p}_m^r \mathbf{g} \mathbf{N} d\Omega$$

$$\mathbf{K}_{1-3} = \int_\Omega \mathbf{B}^T \mathbf{m} \alpha \left(\frac{\partial^2 p_s}{\partial {h_m}^2} \right)^r \dot{h}_m^r \mathbf{N} d\Omega + \int_\Omega \mathbf{B}^T \mathbf{m} \alpha \left(\frac{\partial^2 p_s}{\partial p_m \partial h_m} \right)^r \dot{p}_m^r \mathbf{N} d\Omega + \int_\Omega \mathbf{B}^T \mathbf{m} \alpha \left(\frac{\partial^2 p_s}{\partial s_c \partial h_m} \right)^r \dot{s}_c^r \mathbf{N} d\Omega$$
$$+ \int_\Omega \mathbf{N}_u^T \left(\frac{\partial^2 \rho_{eff}}{\partial {h_m}^2} \right)^r \dot{h}_m^r \mathbf{g} \mathbf{N} d\Omega + \int_\Omega \mathbf{N}_u^T \left(\frac{\partial^2 \rho_{eff}}{\partial p_m \partial h_m} \right)^r \dot{p}_m^r \mathbf{g} \mathbf{N} d\Omega$$

$$\mathbf{K}_{1-5} = \int_\Omega \mathbf{B}^T \mathbf{m} \alpha \left(\frac{\partial^2 p_s}{\partial h_m \partial s_c} \right)^r \dot{h}_m^r \mathbf{N} d\Omega + \int_\Omega \mathbf{B}^T \mathbf{m} \alpha \left(\frac{\partial^2 p_s}{\partial p_m \partial s_c} \right)^r \dot{p}_m^r \mathbf{N} d\Omega + \int_\Omega \mathbf{B}^T \mathbf{m} \alpha \left(\frac{\partial^2 p_s}{\partial {s_c}^2} \right)^r \dot{s}_c^r \mathbf{N} d\Omega$$

$$\mathbf{K}_{1-6} = \int_\Omega \mathbf{B}^T \mathbf{m} \alpha \left(\frac{\partial^2 p_s}{\partial h_m \partial s_c} \right)^r \dot{h}_m^r \mathbf{N}^* d\Omega + \int_\Omega \mathbf{B}^T \mathbf{m} \alpha \left(\frac{\partial^2 p_s}{\partial p_m \partial s_c} \right)^r \dot{p}_m^r \mathbf{N}^* d\Omega$$
$$+ \int_\Omega \mathbf{B}^T \mathbf{m} \alpha \left(\frac{\partial^2 p_s}{\partial {s_c}^2} \right)^r \dot{s}_c^r \mathbf{N}^* d\Omega$$

$$\mathbf{K}_{2-1} = \mathbf{K}_{2-4} = 0$$

$$\mathbf{K}_{2-2} = \int_\Omega \mathbf{N}^T \left(\frac{\partial d_1}{\partial p_m} \right)^r \dot{p}_m^r \mathbf{N} d\Omega + \int_\Omega \mathbf{N}^T \left(\frac{\partial d_2}{\partial p_m} \right)^r \dot{h}_m^r \mathbf{N} d\Omega + \int_\Omega \mathbf{N}^T \left(\frac{\partial d_3}{\partial pm} \right)^r \dot{h}_s^r \mathbf{N} d\Omega$$
$$+ \int_\Omega \mathbf{N}^T \left(\frac{\partial d_4}{\partial p_m} \right)^r \mathbf{m}^T \mathbf{L} \dot{\mathbf{u}}^r \mathbf{N} d\Omega + \int_\Omega \nabla \mathbf{N}^T \cdot \mathbf{c}_1^r \nabla \mathbf{N} d\Omega + \int_\Omega \nabla \mathbf{N}^T \cdot \left(\frac{\partial \mathbf{c}_1}{\partial p_m} \right)^r \nabla p_m^r \mathbf{N} d\Omega$$
$$+ \int_\Omega \nabla \mathbf{N}^T \cdot \left(\frac{\partial \mathbf{c}_2}{\partial p_m} \right)^r \nabla s_c^r \mathbf{N} d\Omega - \int_\Omega \nabla \mathbf{N}^T \cdot \left(\frac{\partial \mathbf{G}_1}{\partial p_m} \right)^r \mathbf{N} d\Omega + \int_\Omega \mathbf{N}^T \left(\frac{\partial e_1}{\partial pm} \right)^r \dot{s}_c^r \mathbf{N} d\Omega$$

$$\mathbf{K}_{2-3} = \int_\Omega \mathbf{N}^T \left(\frac{\partial d_1}{\partial h_m} \right)^r \dot{p}_m^r \mathbf{N} d\Omega + \int_\Omega \mathbf{N}^T \left(\frac{\partial d_2}{\partial h_m} \right)^r \dot{h}_m^r \mathbf{N} d\Omega + \int_\Omega \mathbf{N}^T \left(\frac{\partial d_3}{\partial h_m} \right)^r \dot{h}_s^r \mathbf{N} d\Omega$$
$$+ \int_\Omega \mathbf{N}^T \left(\frac{\partial d_4}{\partial h_m} \right)^r \mathbf{m}^T \mathbf{L} \dot{\mathbf{u}}^r \mathbf{N} d\Omega + \int_\Omega \nabla \mathbf{N}^T \cdot \left(\frac{\partial \mathbf{c}_1}{\partial h_m} \right)^r \nabla p_m^r \mathbf{N} d\Omega$$
$$+ \int_\Omega \nabla \mathbf{N}^T \cdot \left(\frac{\partial \mathbf{c}_2}{\partial h_m} \right)^r \nabla s_c^r \mathbf{N} d\Omega - \int_\Omega \nabla \mathbf{N}^T \cdot \left(\frac{\partial \mathbf{G}_1}{\partial h_m} \right)^r \mathbf{N} d\Omega + \int_\Omega \mathbf{N}^T \left(\frac{\partial e_1}{\partial h_m} \right)^r \dot{s}_c^r \mathbf{N} d\Omega$$

$$\mathbf{K}_{2-5} = \int_\Omega \nabla \mathbf{N}^T \cdot \mathbf{c}_2^r \nabla \mathbf{N} d\Omega + \int_\Omega \mathbf{N}^T \left(\frac{\partial d_1}{\partial s_c} \right)^r \dot{p}_m^r \mathbf{N} d\Omega + \int_\Omega \mathbf{N}^T \left(\frac{\partial d_2}{\partial s_c} \right)^r \dot{h}_m^r \mathbf{N} d\Omega$$
$$+ \int_\Omega \mathbf{N}^T \left(\frac{\partial e_1}{\partial s_c} \right)^r \dot{s}_c^r \mathbf{N} d\Omega$$

$$\mathbf{K}_{2-6} = \int_\Omega \nabla \mathbf{N}^T \cdot \mathbf{c}_2^r \nabla \mathbf{N}^* d\Omega + \int_\Omega \mathbf{N}^T \left(\frac{\partial d_1}{\partial s_c} \right)^r \dot{p}_m^r \mathbf{N}^* d\Omega + \int_\Omega \mathbf{N}^T \left(\frac{\partial d_2}{\partial s_c} \right)^r \dot{h}_m^r \mathbf{N}^* d\Omega$$
$$+ \int_\Omega \mathbf{N}^T \left(\frac{\partial e_1}{\partial s_c} \right)^r \dot{s}_c^r \mathbf{N}^* d\Omega$$

$$\mathbf{K}_{3-1} = 0$$

$$\mathbf{K}_{3-2} = \int_\Omega \mathbf{N}^T \left(\frac{\partial d_5}{\partial p_m}\right)^r \dot{h}_s^r \mathbf{N} d\Omega + \int_\Omega \mathbf{N}^T \left(\frac{\partial d_6}{\partial p_m}\right)^r \dot{h}_m^r \mathbf{N} d\Omega + \int_\Omega \mathbf{N}^T \left(\frac{\partial d_7}{\partial p_m}\right)^r \dot{p}_m^r \mathbf{N} d\Omega$$
$$+ \int_\Omega \mathbf{N}^T \left(\frac{\partial d_8}{\partial p_m}\right)^r \mathbf{m}^T \mathbf{L} \dot{\mathbf{u}}^r \mathbf{N} d\Omega + \int_\Omega \nabla \mathbf{N}^T \cdot \mathbf{c}_3^r \nabla \mathbf{N} d\Omega + \int_\Omega \nabla \mathbf{N}^T \cdot \left(\frac{\partial \mathbf{c}_3}{\partial p_m}\right)^r \nabla p_m^r \mathbf{N} d\Omega$$
$$+ \int_\Omega \nabla \mathbf{N}^T \cdot \left(\frac{\partial \mathbf{c}_4}{\partial p_m}\right)^r \nabla s_c^r \mathbf{N} d\Omega + \int_\Omega \nabla \mathbf{N}^T \cdot \left(\frac{\partial \mathbf{c}_5}{\partial p_m}\right)^r \nabla h_s^r \mathbf{N} d\Omega - \int_\Omega \nabla \mathbf{N}^T \cdot \left(\frac{\partial \mathbf{G}_2}{\partial p_m}\right)^r \mathbf{N} d\Omega$$
$$+ \int_\Omega \mathbf{N}^T \left(\frac{\partial e_2}{\partial p_m}\right)^r \dot{s}_c^r \mathbf{N} d\Omega$$

$$\mathbf{K}_{3-3} = \int_\Omega \mathbf{N}^T \left(\frac{\partial d_5}{\partial h_m}\right)^r \dot{h}_s^r \mathbf{N} d\Omega + \int_\Omega \mathbf{N}^T \left(\frac{\partial d_6}{\partial h_m}\right)^r \dot{h}_m^r \mathbf{N} d\Omega + \int_\Omega \mathbf{N}^T \left(\frac{\partial d_7}{\partial h_m}\right)^r \dot{p}_m^r \mathbf{N} d\Omega$$
$$+ \int_\Omega \mathbf{N}^T \left(\frac{\partial d_8}{\partial h_m}\right)^r \mathbf{m}^T \mathbf{L} \dot{\mathbf{u}}^r \mathbf{N} d\Omega + \int_\Omega \nabla \mathbf{N}^T \cdot \left(\frac{\partial \mathbf{c}_3}{\partial h_m}\right)^r \nabla p_m^r \mathbf{N} d\Omega$$
$$+ \int_\Omega \nabla \mathbf{N}^T \cdot \left(\frac{\partial \mathbf{c}_4}{\partial h_m}\right)^r \nabla s_c^r \mathbf{N} d\Omega + \int_\Omega \nabla \mathbf{N}^T \cdot \left(\frac{\partial \mathbf{c}_5}{\partial h_m}\right)^r \nabla h_s^r \mathbf{N} d\Omega - \int_\Omega \nabla \mathbf{N}^T \cdot \left(\frac{\partial \mathbf{G}_2}{\partial h_m}\right)^r \mathbf{N} d\Omega$$
$$+ \int_\Omega \mathbf{N}^T \left(\frac{\partial e_2}{\partial h_m}\right)^r \dot{s}_c^r \mathbf{N} d\Omega$$

$$\mathbf{K}_{3-4} = \int_\Omega \mathbf{N}^T \left(\frac{\partial d_8}{\partial h_s}\right)^r \mathbf{m}^T \mathbf{L} \dot{\mathbf{u}}^r \mathbf{N} d\Omega + \int_\Omega \nabla \mathbf{N}^T \cdot \mathbf{c}_5^r \nabla \mathbf{N} d\Omega \quad ;$$

$$\mathbf{K}_{3-5} = \int_\Omega \nabla \mathbf{N}^T \cdot \mathbf{c}_4^r \nabla \mathbf{N} d\Omega + \int_\Omega \mathbf{N}^T \left(\frac{\partial d_6}{\partial s_c}\right)^r \dot{h}_m^r \mathbf{N} d\Omega + \int_\Omega \mathbf{N}^T \left(\frac{\partial d_7}{\partial s_c}\right)^r \dot{p}_m^r \mathbf{N} d\Omega$$
$$+ \int_\Omega \mathbf{N}^T \left(\frac{\partial e_2}{\partial s_c}\right)^r \dot{s}_c^r \mathbf{N} d\Omega$$

$$\mathbf{K}_{3-6} = \int_\Omega \nabla \mathbf{N}^T \cdot \mathbf{c}_4^r \nabla \mathbf{N}^* d\Omega + \int_\Omega \mathbf{N}^T \left(\frac{\partial d_6}{\partial s_c}\right)^r \dot{h}_m^r \mathbf{N}^* d\Omega + \int_\Omega \mathbf{N}^T \left(\frac{\partial d_7}{\partial s_c}\right)^r \dot{p}_m^r \mathbf{N}^* d\Omega$$
$$+ \int_\Omega \mathbf{N}^T \left(\frac{\partial e_2}{\partial s_c}\right)^r \dot{s}_c^r \mathbf{N}^* d\Omega$$

$$\mathbf{K}_{4-1} = \mathbf{K}_{4-5} = \mathbf{K}_{4-6} = 0 \quad ; \quad \mathbf{K}_{4-2} = -\int_{\Omega} \mathbf{N}^T \left(\frac{\partial T_m}{\partial p_m} \right)^r \mathbf{N} d\Omega$$

$$\mathbf{K}_{4-3} = -\int_{\Omega} \mathbf{N}^T \left(\frac{\partial T_m}{\partial h_m} \right)^r \mathbf{N} d\Omega \quad ; \quad \mathbf{K}_{4-4} = \int_{\Omega} \mathbf{N}^T \frac{1}{c_{ps}} \mathbf{N} d\Omega$$

$$\mathbf{K}_{5-1} = \mathbf{K}_{5-4} = \mathbf{K}_{5-5} = \mathbf{K}_{5-6} = 0 \quad ; \quad \mathbf{K}_{5-2} = \int_{\Omega} \mathbf{N}^T \left(\frac{\partial f_{sc}}{\partial p_m} \right)^r \mathbf{N} d\Omega$$

$$\mathbf{K}_{5-3} = \int_{\Omega} \mathbf{N}^T \left(\frac{\partial f_{sc}}{\partial h_m} \right)^r \mathbf{N} d\Omega \quad ; \quad \mathbf{K}_{6-1} = \mathbf{K}_{6-4} = \mathbf{K}_{6-5} = \mathbf{K}_{6-6} = 0$$

$$\mathbf{K}_{6-2} = \int_{\Omega} \mathbf{N}^{*T} \left(\frac{\partial f_{sc}}{\partial p_m} \right)^r \mathbf{N} d\Omega \quad ; \quad \mathbf{K}_{6-3} = \int_{\Omega} \mathbf{N}^{*T} \left(\frac{\partial f_{sc}}{\partial h_m} \right)^r \mathbf{N} d\Omega$$

C submatrices

$$\mathbf{C}_{1-1} = -\int_\Omega \mathbf{B}^T \mathbf{D}_s \mathbf{B} d\Omega \quad ; \quad \mathbf{C}_{1-2} = \int_\Omega \mathbf{B}^T \mathbf{m} \alpha \left(\frac{\partial p_s}{\partial p_m} \right)^r \mathbf{N} d\Omega + \int_\Omega \mathbf{N}_u^T \left(\frac{\partial \rho_{eff}}{\partial p_m} \right)^r \mathbf{g} \mathbf{N} d\Omega$$

$$\mathbf{C}_{1-3} = \int_\Omega \mathbf{B}^T \mathbf{m} \alpha \left(\frac{\partial p_s}{\partial h_m} \right)^r \mathbf{N} d\Omega + \int_\Omega \mathbf{N}_u^T \left(\frac{\partial \rho_{eff}}{\partial h_m} \right)^r \mathbf{g} \mathbf{N} d\Omega \quad ; \quad \mathbf{C}_{1-4} = \int_\Omega \mathbf{B}^T \mathbf{D}_s \frac{1}{3} \mathbf{m} \beta_s \frac{1}{c_{ps}} \mathbf{N} d\Omega$$

$$\mathbf{C}_{1-5} = \int_\Omega \mathbf{B}^T \mathbf{m} \alpha \left(\frac{\partial p_s}{\partial s_c} \right)^r \mathbf{N} d\Omega \quad ; \quad \mathbf{C}_{1-6} = \int_\Omega \mathbf{B}^T \mathbf{m} \alpha \left(\frac{\partial p_s}{\partial s_c} \right)^r \mathbf{N}^* d\Omega$$

$$\mathbf{C}_{2-1} = \int_\Omega \mathbf{N}^T d_4^r \mathbf{m}^T \mathbf{B} d\Omega \quad ; \quad \mathbf{C}_{2-2} = \int_\Omega \mathbf{N}^T d_1^r \mathbf{N} d\Omega \quad ; \quad \mathbf{C}_{2-3} = \int_\Omega \mathbf{N}^T d_2^r \mathbf{N} d\Omega$$

$$\mathbf{C}_{2-4} = \int_\Omega \mathbf{N}^T d_3^r \mathbf{N} d\Omega \quad ; \quad \mathbf{C}_{2-5} = \int_\Omega \mathbf{N}^T e_1^r \mathbf{N} d\Omega \quad ; \quad \mathbf{C}_{2-6} = \int_\Omega \mathbf{N}^T e_1^r \mathbf{N}^* d\Omega$$

$$\mathbf{C}_{3-1} = \int_\Omega \mathbf{N}^T d_8^r \mathbf{m}^T \mathbf{B} d\Omega \quad ; \quad \mathbf{C}_{3-2} = \int_\Omega \mathbf{N}^T d_7^r \mathbf{N} d\Omega \quad ; \quad \mathbf{C}_{3-3} = \int_\Omega \mathbf{N}^T d_6^r \mathbf{N} d\Omega$$

$$\mathbf{C}_{3-4} = \int_\Omega \mathbf{N}^T d_5^r \mathbf{N} d\Omega \quad ; \quad \mathbf{C}_{3-5} = \int_\Omega \mathbf{N}^T e_2^r \mathbf{N} d\Omega \quad ; \quad \mathbf{C}_{3-6} = \int_\Omega \mathbf{N}^T e_2^r \mathbf{N}^* d\Omega$$

$$\mathbf{C}_{4-1} = \mathbf{C}_{4-2} = \mathbf{C}_{4-3} = \mathbf{C}_{4-4} = \mathbf{C}_{4-5} = \mathbf{C}_{4-6} = 0$$

$$\mathbf{C}_{5-1} = \mathbf{C}_{5-2} = \mathbf{C}_{5-3} = \mathbf{C}_{5-4} = \mathbf{C}_{5-5} = \mathbf{C}_{5-6} = 0$$

$$\mathbf{C}_{6-1} = \mathbf{C}_{6-2} = \mathbf{C}_{6-3} = \mathbf{C}_{6-4} = \mathbf{C}_{6-5} = \mathbf{C}_{6-6} = 0$$

References

Al-Khoury, R., Sluys, L.J.: A computational model for fracturing porous media. Int. J. Numer. Methods Eng. 70(4), 423-444 (2007).

Amiri, E.A., Craig, J.R., Kurylyk, B.L.: A theoretical extension of the soil freezing curve paradigm. Advances in Water Resources 111, 319-328 (2018).

Anstett, M., Hubbuch, M., Laloui, L., Matthey, B., Morath, M., Pahud, D., Parriaux, A., Rybach, L., Schonbachler, M., Tacher, L.: Utilisation de la chaleur du sol par des ouvrages de foundation et de soutenement en beton, Guide pour la conception, la realisation et la maintenance. Swiss Society of Engineers and Architects (SIA), Documentation D 0190 (2005).

Arzanfudi, M.M., Al-Khoury, R.: Thermo-hydrodynamic-mechanical multiphase flow model for crack propagation in deformable porous media. International Journal for Numerical Methods in Fluids 84, 635-674 (2017).

Bekele, Y.W., Kyokawa, H., Kvarving, A.M., Kvamsdal, T., Nordal, S.: Isogeometric analysis of THM coupled processes in ground freezing. Computers and Geotechnics 88, 129-145 (2017).

Benchikh, O., Fournier, D., Boccara, A., Teixeira, J.: Photothermal measurement of the thermal conductivity of supercooled water. Journal de Physique 46(5), 727-731 (1985).

Brooks, R.H., Corey, A.T.: Hydraulic Properties of Porous Media. Hydrology Papers, Colorado State University(March) (1964).

Caicedo, B.: Physical modelling of freezing and thawing of unsaturated soils. Géotechnique 67(2), 106-126 (2017).

Cooper, J., Dooley, R.: Release of the IAPWS formulation 2008 for the viscosity of ordinary water substance. The International Association for the Properties of Water and Steam (2008).

Coussy, O.: Poromechanics of freezing materials. Journal of the Mechanics and Physics of Solids 53(8), 1689-1718 (2005).

Fukusako, S.: Thermophysical properties of ice, snow, and sea ice. International Journal of Thermophysics 11(2), 353-372 (1990).

Gilpin, R.R.: A model for the prediction of ice lensing and frost heave in soils. Water Resources Research 16(5), 918-930 (1980).

Grenier, C., Anbergen, H., Bense, V., Chanzy, Q., Coon, E., Collier, N., Costard, F., Ferry, M., Frampton, A., Frederick, J., Gonçalvès, J., Holmén, J., Jost, A., Kokh, S., Kurylyk, B., McKenzie, J., Molson, J., Mouche, E., Orgogozo, L., Pannetier, R., Rivière, A., Roux, N., Rühaak, W., Scheidegger, J., Selroos, J.-O., Therrien, R., Vidstrand, P., Voss, C.:

Groundwater flow and heat transport for systems undergoing freeze-thaw: Intercomparison of numerical simulators for 2D test cases. Advances in Water Resources 114, 196-218 (2018).
Guymon, G.L., Luthin, J.N.: A coupled heat and moisture transport model for arctic soils. Water Resources Research 10(5), 995-1001 (1974).
Hallett, J.: The temperature dependence of the viscosity of supercooled water. Proceedings of the Physical Society 82(6), 1046 (1963).
Hare, D., Sorensen, C.: The density of supercooled water. II. Bulk samples cooled to the homogeneous nucleation limit. The Journal of chemical physics 87(8), 4840-4845 (1987).
Harlan, R.: Analysis of coupled heat-fluid transport in partially frozen soil. Water Resources Research 9(5), 1314-1323 (1973).
IAPWS: Revised release on the IAPWS industrial formulation 1997 for the thermodynamic properties of water and steam. In. The International Association for the Properties of Water and Steam, (2007)
Konrad, J.M., Duquennoi, C.: A model for water transport and ice lensing in freezing soils. Water Resources Research 29(9), 3109-3124 (1993).
Kruschwitz, J., Bluhm, J.: Modeling of ice formation in porous solids with regard to the description of frost damage. Computational Materials Science 32(3-4), 407-417 (2005).
Kurylyk, B.L., Watanabe, K.: The mathematical representation of freezing and thawing processes in variably-saturated, non-deformable soils. Advances in Water Resources 60, 160-177 (2013).
Lewis, R.W., Schrefler, B.A.: The finite element method in the static and dynamic deformation and consolidation of porous media. second ed., Wiley, Chichester, 1998**.**
Mikkola, M., Hartikainen, J.: Mathematical model of soil freezing and its numerical implementation. International Journal for Numerical Methods in Engineering 52(5-6), 543-557 (2001).
Ming, F., Zhang, Y., Li, D.-q.: Experimental and theoretical investigations into the formation of ice lenses in deformable porous media. Geosciences Journal 20(5), 667-679 (2016).
Na, S., Sun, W.: Computational thermo-hydro-mechanics for multiphase freezing and thawing porous media in the finite deformation range. Computer Methods in Applied Mechanics and Engineering 318, 667-700 (2017).
Nishimura, S., Gens, A., Olivella, S., Jardine, R.: THM-coupled finite element analysis of frozen soil: formulation and application. (2008).
O'Neill, K., Miller, R.D.: Exploration of a rigid ice model of frost heave. Water Resources Research 21(3), 281-296 (1985).
Ramires, M., de Castro, C.N., Nagasaka, Y., Nagashima, A.: Standard Reference Data for the Thermal Conductivity of Water. (1994).
Sheng, D., Axelsson, K., Knutsson, S.: Frost heave due to ice lens formation in freezing soils: 1. Theory and verification. Hydrology Research 26(2), 125-146 (1995).
Steiner, A., Vardon, P.J., Broere, W.: The influence of freeze–thaw cycles on the shear strength of illite clay. Proceedings of the Institution of Civil Engineers-Geotechnical Engineering 171(1), 16-27 (2017).
Takagi, S.: Segregation freezing as the cause of suction force for ice lens formation. In: Developments in Geotechnical Engineering, vol. 26. pp. 93-100. Elsevier, (1979)
Thomas, H.R., Cleall, P.J., Li, Y., Harris, C., Kern-Luetschg, M.: Modelling of cryogenic processes in permafrost and seasonally frozen soils. Geotechnique 59(3), 173-184 (2009).
Tombari, E., Ferrari, C., Salvetti, G.: Heat capacity anomaly in a large sample of supercooled water. Chemical physics letters 300(5-6), 749-751 (1999).
Wettlaufer, J., Worster, M.G.: Premelting dynamics. Annu. Rev. Fluid Mech. 38, 427-452 (2006).
Williams, P.J., Smith, M.W.: The Frozen Earth: Fundamentals of Geocryology. Polar Record**, first ed.,** Cambridge University Press, New York, 1989.
Zhou, M., Meschke, G.: A three-phase thermo-hydro-mechanical finite element model for freezing soils. International Journal for Numerical and Analytical Methods in Geomechanics 37(18), 3173-3193 (2013).